FACULDADE DE ENGENHARIA DA UNIVERSIDADE DO PORTO

UPWIND - Pendulum-Based Take-off for Autonomous Flying Wings in Airborne Wind Energy Systems

Ana Rita Reimão Couto



Mestrado em Engenharia Eletrotécnica e de Computadores

Supervisor: Fernando Arménio da Costa Castro e Fontes

Co-supervisor: Luís Tiago de Freixo Ramos Paiva

October 31, 2024

Resumo

Para enfrentar a questão das alterações climáticas, é crucial descobrir soluções sustentáveis que utilizem recursos naturais para gerar energia renovável, em vez de depender de combustíveis fósseis.

Atualmente, 80 por cento da produção mundial de energia ainda provém do uso de combustíveis fósseis. Para combater este problema, cientistas e investigadores estão a explorar várias formas de reduzir a pegada de carbono e promover a utilização de fontes de energia renováveis. Uma dessas soluções é a utilização de recursos naturais, como o vento, que é uma fonte de energia abundante, económica e sustentável. O uso da energia eólica apresenta diversas vantagens em relação às fontes de energia convencionais, como redução de emissões de gases de efeito estufa, baixo custo operacional e mínimo impacto ambiental. A energia eólica é um recurso natural valioso que pode ser obtido por meio de turbinas e *Airborne Wind Energy Systems* (*AWES*).

Existem vários projetos e grupos de investigação dedicados ao estudo desta inovadora tecnologia nos quais podemos destacar o projeto *UPWIND*.

O projeto *UPWIND* tem como foco a pesquisa e desenvolvimento de *AWES* (*Airborne Wind Energy Systems*) que utilizam uma asa ou *kite*, um cabo e um gerador para produzir energia por meio de tração em grandes altitudes. O objetivo é servir como um complemento às turbinas eólicas tradicionais, que são atualmente a fonte de produção de energia eólica mais utilizada no mundo. No entanto, como esta tecnologia ainda se encontra numa fase inicial, existem muitos desafios a serem enfrentados em termos de aspetos económicos, eficiência e segurança.

Uma das tarefas mais importantes e também um das mais desafiante é o desenvolvimento de um controlador automático de descolagem que consiga operar em quaisquer condições e de forma confiável.

O objetivo principal desta tese foca-se em desenvolver um controlador automático de descolagem baseado no movimento pendular que seja capaz de operar de forma autónoma sem intervenção humana, resultando em maior eficiência. No entanto, o desenvolvimento de um sistema de descolagem automático apresenta vários desafios de controlo, como o controlo de parâmetros de forma a garantir a estabilidade do *kite* desde o seu lançamento até todas as fases do ciclo de voo.

Este documento apresentará estudos e várias simulações de vários problemas de diferentes complexidades. Simulações que servirão como meio de estudo e análise da viabilidade deste tipo de descolagem.

Abstract

To tackle the issue of climate change, it is crucial to discover sustainable solutions that utilize natural resources to generate renewable energy instead of relying on fossil fuels. Currently, around 80 percent of the energy of the world is still sourced from fossil fuels.To combat this issue, scientists and experts are exploring various ways to reduce the carbon footprint and promote the use of renewable energy sources. One such solution is the use of natural resources, such as wind, which is an abundant, economical, and sustainable source of energy. The use of wind energy has several advantages over conventional energy sources, such as reduced greenhouse gas emissions, low operational cost, and minimal environmental impact. Wind energy is a valuable natural resource that can be obtained using turbines and Airborne Wind Energy Systems (AWES).

There are numerous projects and research groups dedicated to exploring this groundbreaking technology, such as the UPWIND project.

The UPWIND project focuses on researching and developing AWES (airborne wind energy systems) that use a wing or kite, a cable, and a generator to produce energy through traction at high altitudes. The aim is to complement traditional wind turbines, currently the most commonly used source of wind energy production worldwide. However, as this technology is still in its early stages, there are many challenges to be addressed in terms of economic aspects, efficiency, and safety.

One of the most important and challenging tasks is to develop a reliable automatic take-off controller that can operate in all conditions.

The main objective of this thesis is to develop an automated take-off controller that uses pendulum movement to launch a kite. The mechanism should be capable of starting and completing the take-off process without human intervention, resulting in improved efficiency. However, the development of an automatic take-off mechanism presents several control challenges to ensure the stability of the kite from the beginning of the launch to the end of the flight cycle.

This document will feature several studies and simulations of various issues of different complexities. These simulations will serve as a means of studying and analyzing the feasibility of this type of take-off.

Sustainable Development Goals (SDG) of the United Nations

In 2015, all member states of the United Nations committed to the 2030 Agenda for Sustainable Development. This plan aims to achieve peace and address threats to people and the planet and was adopted by both developed and developing countries. The 2030 Agenda provides a universal framework for achieving sustainable development in the future [1].

There are 17 Sustainable Development Goals (SDGs)(1) that are urgent calls for action by all countries, poor, rich, and middle-income, in order to guarantee the prosperity and protection of people and the plane [1].



Figure 1: The 17 Sustainable Development Goals (SDGs) (Source: [1])

Since the creation of these 17 goals, 3,906 events, 1,348 publications, and 7,842 actions have been carried out for 169 targets. All countries belonging to the Member States of the United Nations confirm that the fight against poverty, hunger, climate change, and other deprivations must go hand in hand with strategies to improve health and education, reduce inequalities, maintain economic growth, combat climate change, and protect oceans and forests [1].

Engineering plays a crucial role in achieving the 17 SDGs, promoting equality, and ensuring a balanced and inclusive profession for all genders.

This thesis aims to create an automated control system for the take-off process of the UPWIND project. The UPWIND project aims to harness sustainable wind energy as a green alternative to the conventional turbine-based approach, which is currently the dominant mode of wind energy production. While the thesis does not explicitly address any of the 17 United Nations Sustainable Development Goals (SDGs), it is closely linked to them. By analyzing the project context, it is possible to identify several SDGs to which the project contributes. The table below highlights the SDGs achieved by the project, along with specific objectives and performance indicators to measure the degree of success in achieving these goals.

Airborne Wind Energy involves using natural resources, like wind, to generate electricity in a clean and sustainable way. Airborne Wind Energy is a method of harnessing energy from the wind by employing a wing or kite, a cable, and a generator. This process occurs at high altitudes, where control and technology are utilized to maximize sustainability and green energy production. The production of green energy is becoming increasingly important for reducing the use of fossil fuels and reducing the carbon footprint.

Table 1 illustrates several Sustainable Development Goals (SDGs) established by the United Nations, which provide a framework for integrating Airborne Wind Energy into the existing energy infrastructure. As such, the objective of this thesis can be integrated into the same goals.

Table 1: Contribution to SDGs and Performance Indicators

SDG	**Target**	**Contribution**	**Performance Indicators and Metrics**
7	7.1	Increase the proportion of renewable energy within the global energy composition	Indicator 7.1.1: Proportion of renewable energy in the overall final energy consumption.
	7.2	Improve energy efficiency by harnessing high-altitude winds with AWES.	Indicator 7.2.1: Energy intensity, measured by the ratio of primary energy consumption to gross domestic product (GDP) (an indicator of energy efficiency and economic output).
9	9.1	Embrace clean and sustainable technologies like AWES to reduce carbon emissions.	Indicator 9.1.1: CO2 emission per unit of value added.
	9.2	Enhance technological and research capacity through the development of AWES.	Indicator 9.2.1: Research and development expenditure as a proportion of GDP.
11	11.1	Minimize the environmental effects of urban areas by integrating AWES.	Indicator 11.1.1: Annual average levels of fine particulate matter (PM2.5 and PM10) in urban areas.
	11.2	Promote the development of green and public spaces indirectly by reducing reliance on traditional energy infrastructure.	Indicator 11.2.1: Average proportion of public open space in urban built-up areas.
13	13.1	Enhance resilience to natural disasters.	Indicator 13.1.1: Number of countries with national and local disaster risk reduction strategies.
	13.2	Enhance education and build institutional capacity for addressing climate change through AWES-related training and research..	Indicator 13.2.1: Number of countries that have integrated mitigation, adaptation, impact reduction, and early warning into primary, secondary, and tertiary curricula

Agradecimentos

I would like to express my deepest appreciation to my supervisor, Fernando Arménio da Costa Castro e Fontes, and co-supervisor, Luís Tiago de Freixo Ramos Paiva, for their invaluable support and guidance during this phase of my research. This initial journey would be much more challenging without their invaluable expertise and guidance.

I want to express my gratitude to Professor Luís Augusto Correia Roque for his invaluable assistance throughout this challenging process. He helped me with a wide range of questions, from coding issues to theoretical inquiries.

I would like to express my gratitude to my colleagues of the LSCOE (Laboratory of Systems, Control, Optimization, and Estimation) SYSTEC-ARISE located in Lab i202 DEEC-FEUP, particularly Sérgio Vinha, Gabriel Fernandes, Rui Costa, and Manuel Fernandes, for sharing their valuable advice based on their personal experiences. Their support has been crucial in shaping and refining my work.

To my friends who have been part of my journey and who have always supported me and helped me through the most complicated and stressful times, always with words of comfort and support. Especially Ana Catarina, without a doubt, this journey would not have been the same without you.

I want to extend my heartfelt thanks to my mother, Maria da Conceição de Jesus Reimão, and my father, Manuel Carlos Martins Couto, for their unwavering support and guidance. Their presence and encouragement have been my source of strength and motivation, especially during times when I felt lost and unsure. Their belief in me has been a driving force behind my success, and I am truly grateful for their unwavering support.

Finally, I want to thank the financial support by national funds through the FCT/MCTES (PIDDAC) under projects KEFCODE-Algoritmos para Optimização e Configuração de Paques Eólicos com Kites 2022.02320.PTDC, SYSTEC–Research Center for Systems and Technologies.

Ana Rita Reimão Couto

"Success is not final, failure is not fatal: it is the courage to continue that counts."

Winston Churchilll

Contents

Goals of Sustainable Development (SDG) of the United Nations iii

Agradecimentos v

1 Introduction 1
- 1.1 Context and Motivation . . . 1
- 1.2 Challenges, Goals and Starting Point . . . 2
- 1.3 Contributions . . . 2
- 1.4 Dissertation Structure . . . 2

2 Airborne Wind Energy Systems 4
- 2.1 Historical Evolution . . . 4
- 2.2 Economic Aspects . . . 5
- 2.3 Basic Concepts . . . 6
- 2.4 Crosswind Kite Power . . . 7
- 2.5 Classification of Airborne Wind Energy Systems . . . 9
- 2.6 Automatic Take-off and Landing . . . 10
  - 2.6.1 Vertical take-off and landing . . . 11
  - 2.6.2 Linear or catapult take-off and landing . . . 12
  - 2.6.3 Circular take-off and landing . . . 14
  - 2.6.4 Comparison and Viability of Take-off and Landing Methods . . . 15
- 2.7 UPWIND Project . . . 16
  - 2.7.1 Prototype . . . 16
  - 2.7.2 Forces Diagram . . . 18

3 Simple Pendulum System 24
- 3.1 Preliminary Work . . . 24
  - 3.1.1 Problem Description . . . 24
  - 3.1.2 Results and Discussion . . . 25

4 Kite Model 30
- 4.1 Coordinate System . . . 30
- 4.2 Kite Model . . . 32
  - 4.2.1 2D Dimensions . . . 32
  - 4.2.2 3D Dimensions . . . 51

5 Wind Farms 58

6 Conclusions and Future Work **64**
6.1 Conclusions 64
6.2 Future Work 65

References **66**

List of Figures

1 The 17 Sustainable Development Goals (SDGs) (Source: [1]) iii

2.1 Examples of institutions and companies that are working with AWE technology. (Source: [2]) 5
2.2 Potential cost reduction of AWES. (Source: [3]) 5
2.3 Comparing the production potential of AWES with turbines. (Source: [3]) 6
2.4 Examples of AWES (Airborne Wind Energy Systems) which use two different types of generators - a ground generator (a) and a flying generator (b). (Source: [4]) 7
2.5 Traditional turbine (left) and a flying kite or wing in drag mode (right). (Source: [5]) 7
2.6 Various classifications of AWE (Airborne Wind Energy) technologies. (Source: [6]) 9
2.7 Different approaches taken by various companies and research groups. (Source: [7]) 10
2.8 Power conversion for different systems. (Source: [8]) 10
2.9 KiteMill prototype. (Source: [9]) 11
2.10 TwingTec prototype. (Source: [10]) 12
2.11 Makani prototype. (Source: [11]) 12
2.12 Ampyx Power prototype. (Source: [12]) 13
2.13 ElektRail prototype. (Source: [13]) 13
2.14 Fully automatic experimental circular take-off and landing. (Source: [14]) 14
2.15 EnerKite prototype.(Source: [15]) 14
2.16 Prototype of the large kite. 17
2.17 Prototype of the small kite. 17
2.18 (a) The system coordinates for 2D are visible; (b) The forces diagram on the 2D kite is depicted; (c) The system coordinates and wind direction are shown for 2D purposes. 19
2.19 The system coordinates used for 3d simulation. 20
2.20 Visual representation of the kite in the yz plane. (Source: [16]) 21
2.21 Visual representation of the kite in the xz plane and velocity vector. 21
2.22 Visual representation of the forces acting on the kite in the plane yz. (Source: [16]) 22
2.23 Visual representation of the forces on the plane xz. 23
2.24 Kite Body coordinates (left); Body coordinates diagram representation (right). (Source: [16]) 23

3.1 Simple pendulum - initial position (a) and forces acting on the body of mass during its trajectory (b). (Source: [17]) 25
3.2 Animation of the pendulum motion for mass 1kg. 26
3.3 The trajectory of the motion of the pendulum for mass 1kg. 26
3.4 Graphic of the variation of the angle θ through time for mass 1kg. 27
3.5 Animation of the pendulum motion for mass m kg. 27

3.6 The trajectory of the motion of the pendulum for mass m kg. 28
3.7 Graphic of the variation of the angle θ through time for mass m kg. 28

4.1 Global and Local coordinate systems. 31
4.2 Global and Local coordinate systems used in UPWIND. (Source: [14]) 31
4.3 Body Coordinate Systems. (Source: [18]) 31
4.4 Forces Diagram. 32
4.5 Vector y. 43
4.6 Graph showing the kite dynamic over time. 45
4.7 Graph showing the angular velocity of the kite over time. 45
4.8 Graph displaying the results of changing the angle β in degrees. 46
4.9 Graph showing the kite dynamic over time in response to the wind in favor. . . . 47
4.10 Graph showing the angular velocity of the kite over time in response to the wind in favor in deg/s. 48
4.11 Graph showing the impact of the favor wind on the change in angle β in degrees. 48
4.12 Graph showing the angular velocity of the kite over time in response to the opposing wind in deg/s. 49
4.13 Graph showing the impact of the opposing wind on the change in angle β in degrees. 50
4.14 Visual representation of the kite in the yz plane. (Source: [16]) 51
4.15 Visual representation of the forces on the plane xz. 52
4.16 Visual representation of the forces acting on the kite in the plane yz. (Source: [16]) 53
4.17 Kite circular trajectory within the tangent plane. 55
4.18 Body coordinates System (Source: [16]) 55

5.1 Turbines disposition. (Source: [19] 60
5.2 (i) Disjoint ground areas 60
5.3 (ii) Disjoint workspace cones 60
5.4 (iii) Intersecting workspace cones 60
5.5 AWES sharing a common space. (Source: [19]) 60
5.6 Kite disposition in a Wind Farm using a rectangular layout. (Source: [19] 61
5.7 Distance 1 and 3. 61
5.8 Distance 2. 61
5.9 Distances. (Source: [19]) 61
5.10 Table with data from the studies of the UPWIND project. 62
5.11 Calculating distances for the presented data. 63

List of Tables

1 Contribution to SDGs and Performance Indicators iv

Abbreviations and Symbols

AWES	Airborne Wind Energy Systems
AWE	Airborne Wind Energy
ATOL	Automatic Take-off and Landing
TOL	Take-off and Landing
VTOL	Vertical Take-off and Landing
HTOL	Linear or Catapult Take-off and Landing
CTOL	Circular Take-off and Landing
LCOE	Levelized cost of electricity
2D	Two Dimensions
3D	Three Dimensions
F_g	Gravitational Force (N)
F_P	Push Force (N)
F_D	Drag Force (N)
F_L	Lift Force (N)
F_i	Inertial Forces (N)
F_t	Tangential Force (N)
G	Global coordinate system
L	Local coordinate system
B	Body coordinate system
x, y, z	Cartesian coordinates
ODE	Ordinary Differential Equation
DAEs	Differential Algebraic Equation
r, ϕ, β	Coordinate in spherical local frame
$e_{roll}, e_{pitch}, e_{yaw}$	Body coordinate frame axes
e_1, e_2, e_3	Body coordinate frame axes
$\vec{e}_x, \vec{e}_y, \vec{e}_z$	Reference global frame axes
$\vec{e}_r, \vec{e}_\phi, \vec{e}_\beta$	Reference local frame axes
R	Radius of curvature (m)
g	Gravitational acceleration (ms^{-2})
ρ	Air density (kgm^{-3})
A	Kite Wing Area (m^2)
C_D	Aerodynamic drag coefficient
C_L	Aerodynamic lift coefficient
v_w	Wind velocity (ms^{-1})
v_a	Apparent wind speed (ms^{-1})
v_0	Initial Velocity (ms^{-1})
w	Angular Velocity ($rads^{-1}$))
L	Tether length (m)

Abbreviations and Symbols

P	Kite position (m)
$\dot{P}$	Kite velocity (ms^{-1})
$\vec{v}$	Velocity vector (ms^{-1})
k	Unit vector in the rotation matrix
d_1	Distance between two points aligned with the wind velocity (m)
d_2	Minimum distance between units (m)
d_3	Space between the last unit and the edge of the terrain in each column (m)
d	Maximum distance (m)
L_{max}	Maximum tether length (m)
b	Wind length (m)

Angles

γ	Flight path angle (rad)
ϕ	Roll angle (rad)
β_0	Initial β (rad)
θ	Pitch angle (rad)
α	Cone opening in the yz plane (rad)
σ	Angle between the kite and the x-axis in the xz plane (rad)
$\Delta\beta$	Variation of β
$\Delta\phi$	Variation of ϕ

Chapter 1

Introduction

In the introduction chapter, this dissertation provides an initial contextualization of the problem that will be addressed and the scientific area in which it is situated. It discusses the challenges and motivations behind the problem and highlights the possible applications and implications of solving it. Finally, the chapter briefly mentions the structure of the dissertation.

1.1 Context and Motivation

Even though there have been advancements in renewable energy sources, approximately 80 percent of global energy production still relies on fossil fuels. This highlights the need to explore alternative energy sources more than ever before. Scientists and experts are currently looking into various ways to reduce the carbon footprint and increase the use of renewable energy.

An effective solution is to utilize natural resources, such as wind power. Wind energy is an abundant, economical, and sustainable source of energy. It has several advantages over conventional energy sources, such as lower greenhouse gas emissions, lower operational costs, and minimal environmental impact. Wind energy is a valuable natural resource that can be obtained using turbines and Airborne Wind Energy Systems (AWES).

The UPWIND project focuses on researching and developing AWES that use a wing or kite, a cable, and a generator to produce energy through traction at high altitudes. The primary objective of this project is to provide a complementary solution to traditional wind turbines, which are currently the most commonly used source of wind energy production worldwide.

These systems are still in the development and research phase. However, their unique characteristics allow them to compete with traditional turbines commercially.

These systems differ from traditional turbines due to their unique ability to operate at high altitudes where winds are strong.

To ensure the highest level of efficiency, it is imperative to have an automatic take-off control system. This system eliminates the need for human involvement during the take-off and the entire flight process. Developing an automatic take-off system is crucial for the advancement of these devices, even though it is a challenging task.

1.2 Challenges, Goals and Starting Point

Developing a system that can autonomously perform take-off presents several challenges. It can be challenging to maintain control of a kite during take-off, particularly in adverse weather conditions or system failure. Making the wrong decision can cause damage to the kite, which can be costly and time-consuming to repair. Therefore, it is crucial to create an automatic take-off system that enables autonomy, efficiency, and protection against adversity. Various take-off methods can be used, each with its unique set of challenges in terms of controlling parameters. The UPWIND project is exploring alternative and innovative methods that have great potential to bring about significant advancements, such as take-off based on a pendulum movement. However, there are also major control problems that need to be addressed. One of the first challenges in kite energy production is to ensure that the kite follows a pendulum trajectory with a push force only in the positive velocity direction until it reaches a safe speed for take-off. This will allow the kite to move into the energy production phase smoothly and securely. This control challenge represents one of the starting points for the beginning of this dissertation. In addition to controlling the trajectory, controlling certain kite parameters and the forces present on the kite also poses a challenge that requires further investigation. Despite these challenges, the potential of these wind energy systems to generate more energy than traditional wind turbines has inspired researchers to further develop and optimize this embryonic technology to harness the vast power of the wind.

1.3 Contributions

This thesis introduces a new concept for take-off using pendulum movement, where the aircraft is suspended on a structure until it gains enough speed to begin flying and generating energy. This groundbreaking technology has the potential to transform disused structures, such as turbine towers, into sources of energy production, offering an environmentally friendly and cost-effective solution. The research presented in this thesis provides a foundation for further investigation of this approach in the future, covering both 2D and 3D aspects as well as theoretical and mathematical considerations.

1.4 Dissertation Structure

In addition to the introduction, this dissertation contains 5 more chapters. Chapter 2 provides an overview of the state of the art in Airborne Wind Energy Systems, including historical and economic aspects. It explains the fundamental concepts of this emerging technology, the classification of these systems, and the kite model that will be the focus of the research. The chapter also discusses the different options for take-off and landing, their respective advantages and disadvantages, and the approach chosen by the UPWIND group. In Chapter 3, we will provide an overview of a simpler problem - the pendulum motion of a simple pendulum. This will help us understand

the mathematical, dynamic, and physical foundations, and then progress to a more complex problem. Chapter 4 will present two problems with different complexities. The first problem will be a 2D problem involving the influence and non-influence of wind, along with its implementation and results. Following that, the more complex 3D problem will be presented providing its mathematical and theoretical analyses. Chapter 5 will offer a brief overview of one of the many applications of take-off and its significance in controlling multiple kites in Wind Farms. In Chapter 6, the conclusion and a plan for future steps will be presented.

Chapter 2

Airborne Wind Energy Systems

To provide a comprehensive understanding of the problem presented in this report, this chapter shall offer a detailed account of the theoretical and historical perspectives, as well as the fundamental mathematical and physical concepts that are central to the specific field in which this dissertation is situated.

2.1 Historical Evolution

Before delving into theoretical and physical aspects, it is important to understand the origin of using kites to generate energy. During the energy crisis of the 1970s, there was a growing interest in using natural resources to produce energy. In 1975, Payne and McCutchen patented the “Self-Erecting Windmill” which laid the concepts for the principles of airborne wind energy [14]. Although the idea was introduced earlier, the first person to conduct serious research on this topic was the American engineer Miles L. Loyd. His research led to an article titled "Crosswind Kite Power," which was published in "The Journal of Energy" in 1980 [20]. Therefore, it is safe to say that Miles Loyd was the pioneer of the foundation for quantitative analysis of AWE systems. In the book "Airborne Wind Energy: An Overview of the Technological Approaches", it is also pointed out that this field is based on George Pocock’s book, which describes 19th-century kite-drawn carriages. For over four decades now, the Danish three-blade wind turbine has remained a highly sought-after method for generating wind energy. However, in recent times, commercial entities such as MakaniPower and WindLift have started exploring Airborne Wind Energy Systems for commercial purposes. Additionally, academic institutions globally have been at the forefront of researching this exciting technology, with the aim of contributing to a cleaner and more sustainable future (Figure 2.1).

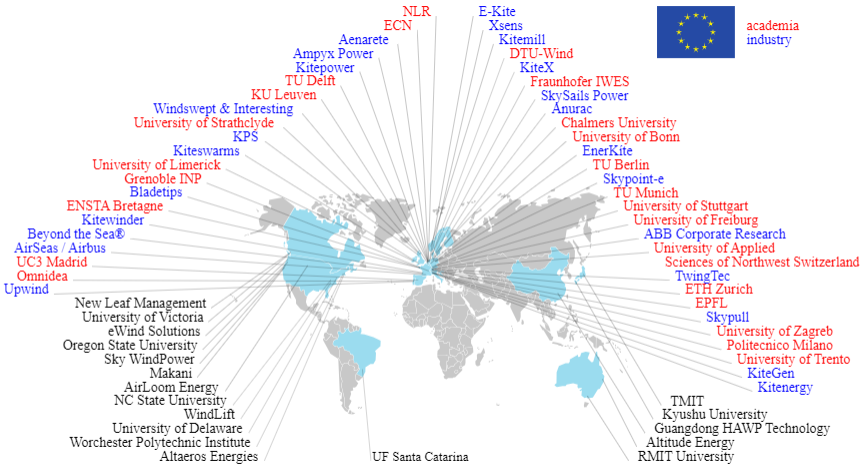


Figure 2.1: Examples of institutions and companies that are working with AWE technology. (Source: [2])

2.2 Economic Aspects

Airborne Wind Energy is a relatively new technology. Therefore, when comparing the market price for low production, the costs may seem high. However, this technology has the potential to not only reduce costs but also increase production significantly [3]. One of its advantages is the ability to fly at high altitudes where the winds are stronger. Figure 2.2 shows a graph that demonstrates the potential of AWES to reduce costs and increase profits. It is estimated that by 2040, AWES will become competitive in the energy market [3].

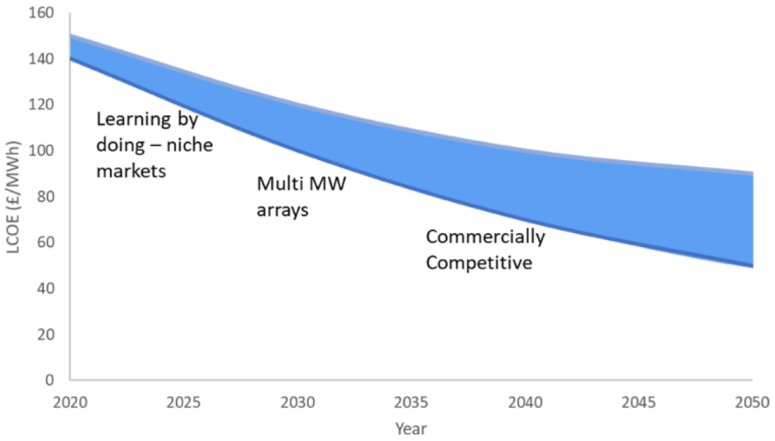


Figure 2.2: Potential cost reduction of AWES. (Source: [3])

Increasing Power and Reduction Cost

When we discuss wind energy, we usually think of turbines as the means of energy production. The amount of energy produced by turbines is directly proportional to the size of their blade area. Therefore, by doubling the blade area, we can quadruple the energy production [3]. However, there is a limit to which the blade can increase, or the tower can grow to reach higher altitudes. This is where Airborne Wind Energy Systems come into play. They can reach greater heights and cover much larger areas, thereby increasing energy production [3]. In figure 2.3, you can see a graph comparing the production potential of AWES to traditional turbines.

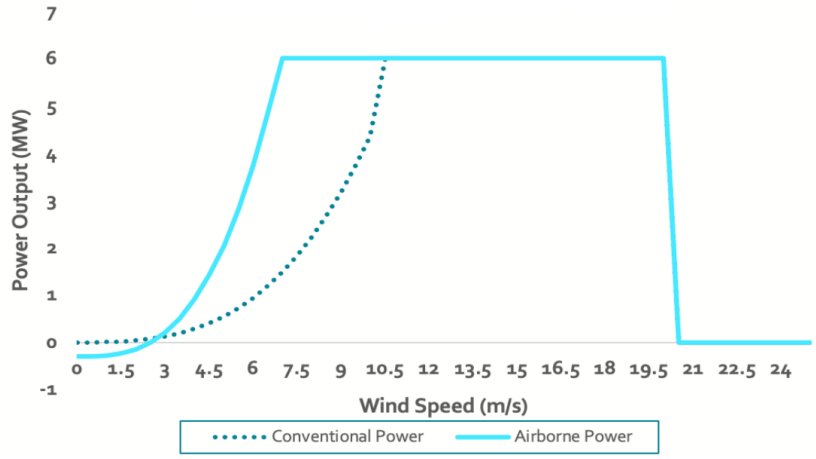


Figure 2.3: Comparing the production potential of AWES with turbines. (Source: [3])

When we use kites or wings, we can enjoy a range of benefits. Firstly, we can increase energy production while making the landscape more aesthetically pleasing. Additionally, there is a reduction in material and maintenance costs. As the costs of materials like steel continue to rise, building a turbine involves many associated costs, both in terms of maintenance and installation or construction [3]. A kite or wing requires less mass than a turbine, making it lighter and easier to install. An Airborne Wind Energy System generator is much smaller than a turbine generator. When it comes to maintenance, AWES technology replaces turbines, and maintenance costs would be mainly associated with the system itself and periodic replacements of the cable and the kite or wing [3]. Overall, we can say that with the growth and entry into the energy market, Airborne Wind Energy Systems have the potential to become one of the most reliable and economically developed forms of energy production.

2.3 Basic Concepts

Airborne Wind Energy Systems (AWES) differ from traditional three-bladed turbines in their approach to generating power. Unlike turbines which have height limitations and are fixed on the ground, AWES can "either fly freely in the air or be connected to the ground by a tether, such as

kites or tethered balloons" [5], and can fly at high altitudes. Mechanically connected AWES can generate more power than those that are not, exploring the "relative velocity between the airmass and the ground" [5]. This approach allows us to fully harness the power of the wind. These systems are connected to a stationary ground station or any type of moving object that is non-flying and can generate power in the form of a traction force to a moving vehicle or in the form of electricity (Figure 2.4). The UPWIND project uses a ground-connected kite approach with a stationary ground station.

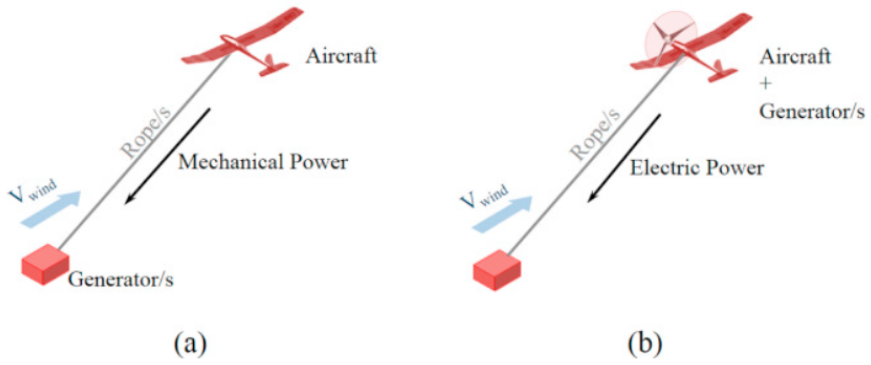


Figure 2.4: Examples of AWES (Airborne Wind Energy Systems) which use two different types of generators - a ground generator (a) and a flying generator (b). (Source: [4])

2.4 Crosswind Kite Power

As we previously stated the concept of Airborne Wind Energy Systems (AWES) involves using a kite or a wing, a cable, and a generator to produce energy from the wind. The research conducted by Miles Loyd proposed a unique method of generating power using airfoils tethered to a cable and flying perpendicular to the wind direction (crosswind) [5]. Flying crosswind and at higher altitudes allows to maximize the energy production of the kite. Miles Loyd stated that the blades of the turbine were the most aerodynamic part [14], which led him to design and patent a system consisting of a kite-like wing connected to a cable anchored to a ground station. This system allows for simulating turbine movement at higher altitudes, without the structure (Figure 2.5).

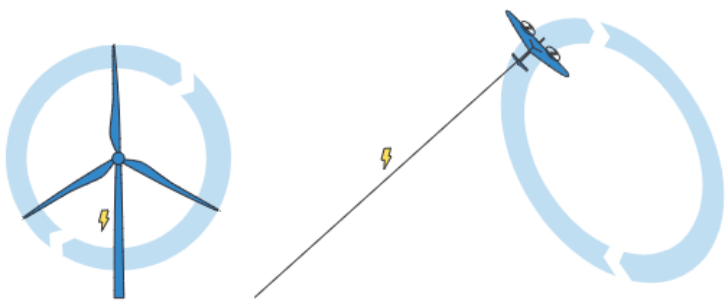


Figure 2.5: Traditional turbine (left) and a flying kite or wing in drag mode (right). (Source: [5])

In his study, he suggested two power conversion modes, the lift mode and the drag mode, which nowadays are the most used and studied ones. The lift mode uses "the tension in the line to pull a load on the ground, the drag mode uses the high apparent airspeed to drive a small wind turbine on the wing" [5]. In the book "Airborne Wind Energy" authored by Ahrens, the estimation of power generation P by a tethered airfoil in both drag and lift modes is discussed. The estimation was made under idealized assumptions and can be approximately given by:

$$P = \frac{2}{27} \cdot \rho \cdot A \cdot v_w^3 \cdot C_L \cdot \left(\frac{C_L}{C_D} \right)^2 \tag{2.1}$$

For AWE systems, the $(\frac{C_L}{C_D})^2$ wing property is a crucial factor for describing aerodynamic efficiency in specific flight conditions, where A represents the wing area, C_L and C_D represent the lift and drag respectively, ρ the air density and v_w the wing speed [5].

When flying at high altitudes in crosswind conditions, we have the perfect conditions to generate maximum power. This can be demonstrated by the following equation:

$$P_{\max} \leq \frac{2}{27} \cdot \rho \cdot A \cdot v_w^3 \cdot C_L \cdot \left(\frac{C_L}{C_D} \right)^2 \cdot (\cos \gamma)^3 \tag{2.2}$$

This formula demonstrates the maximum power that a kite can produce using the same variables as the equation 2.1. It also includes an additional parameter, $(\cos \gamma)^3$, which represents the "angle between the wind velocity vector and the vector pointing along a straight tether from the attachment point on the ground to the aircraft", as explained in the source [14].

This equation differs from the previously presented equation (2.1) in that the energy generated now accounts for the angle γ (the angle between the wind velocity vector and the straight tether connecting the kite or aircraft to the ground). In the earlier formulation, this angle was disregarded under the assumption of ideal conditions, where the wind direction and the tether were perfectly aligned. By incorporating the γ angle, we introduce a more realistic factor, allowing for a more practical estimate of the power that can be generated under real-world flight conditions. The angle γ varies depending on the flight path of the kite, and as such, the term $(\cos \gamma)^3$ becomes crucial in accurately estimating energy production. This adjustment reflects the fact that, in non-ideal conditions, the effective wind speed available to the system is reduced when the wind direction deviates from the tether alignment.

Back in the 1970s and 1980s, the research and ideas related to wind energy seemed impossible due to the lack of technology available at the time. However, with advancements, comprehending and testing wind energy ideas is easier, leading to further improvements and evolution of this technology.

2.5 Classification of Airborne Wind Energy Systems

We can divide AWES into two types, electricity generation (based on the position of the station) and flying operation (crosswind, rotational, or tether-aligned). In figure 2.6, we can see the classification of these systems and the approaches used by different companies or groups.

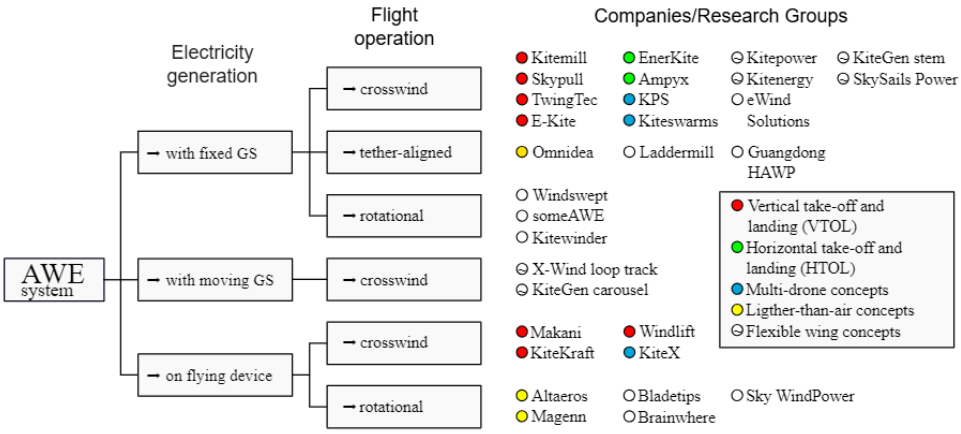


Figure 2.6: Various classifications of AWE (Airborne Wind Energy) technologies. (Source: [6])

Different companies or research groups use different approaches to solve problems. Even within the same category, the solutions found can be significantly different. For example, in the vertical take-off and landing category, we may have solutions where the kite takes off in a vertical line similar to a drone (such as TwinTec). Whereas, in the take-off and landing horizontal solutions, the kite may take-off in a circular trajectory (such as EnerKite) or in a horizontal line where a track is required (such as Ampyx).

When discussing the generation of energy, it is important to consider certain aspects. If the generator is located on the device itself, the energy is generated and then transmitted through a cable. However, if the generator is located in a stationary or mobile station the energy is produced during the reel-out phase when the cable is unwound, and it is consumed during the reel-in phase when the cable is being wound. When we take into account what is produced and consumed, the energy produced exceeds the energy consumed, resulting in a positive balance [18].

In figure 2.7, we can observe the different approaches taken by various companies and research groups.

It is relevant to note that the stability of a wing or kite is also affected by the type of material it is made of. A wing or kite constructed with a more rigid material provides greater control and durability, but it is heavier and more expensive to fix in case of accidents. On the other hand, a wing or kite made of lightweight material is more challenging to control and requires more maintenance, but it is less expensive and easier to repair if damaged [14].

In figure 2.8, we can observe how the location of the generating station and the type of material of the wing or kite affect energy conversion.

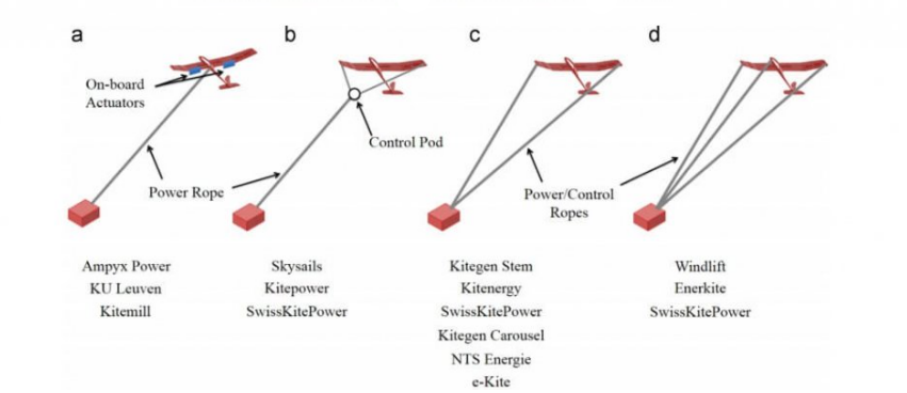


Figure 2.7: Different approaches taken by various companies and research groups. (Source: [7])

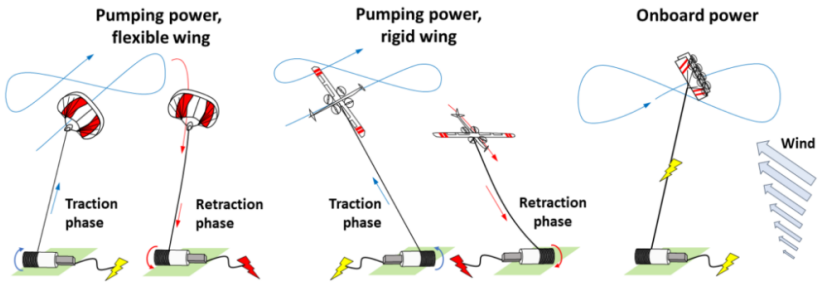


Figure 2.8: Power conversion for different systems. (Source: [8])

Airborne Wind Energy Systems can be classified based on their flight operations. The most commonly used approach is to fly in a crosswind direction, which is perpendicular to the wind. However, this method presents great difficulty in controlling the kite or the parameters of the wing [14]. The choice of flight operation is dependent on the location of the energy generator. Depending on the location of the generator, we may have to use a specific type of flight operation. For example, as shown in figure 2.6, when we have a moving generator station, we need to use the crosswind flight operation. There are also cases where we can choose from three available flight operations. Some companies or research groups prefer to use rotational or tether-aligned flight operations, rather than the crosswind method.

2.6 Automatic Take-off and Landing

Controlling the transitions between take-off and landing is crucial in an Airborne wind Energy System. This allows the system to switch between rest and energy production phases, as well as transition from energy production to immobility phase. The parameters of the kite need to be controlled to ensure that it makes the right decisions during normal situations, extreme weather conditions, or system failures [14]. This is one of the many challenges faced during take-off and landing in such a system.

This thesis introduces a novel take-off method based on a pendulum movement. This method integrates features of both vertical and circular take-off methods. It demonstrates vertical characteristics as the motion takes place in the vertical plane, similar to vertical take-off. Once the kite gains enough speed, it switches from a pendulum-like motion to a circular trajectory, resembling the behavior observed in circular take-off.

The landing of the kite after the energy production phase requires careful consideration, especially in light of the innovative approach proposed in this thesis. It is a crucial aspect of the operation of the system and will be important to consider in future studies to ensure that this take-off method is both reliable and feasible.

Currently, three main approaches are used for take-off and landing in airborne wind energy systems: vertical take-off and landing (VTOL), horizontal or catapult-assisted take-off and landing (HTOL), and circular take-off and landing (CTOL).

In the upcoming subsection, we will examine the advantages and disadvantages of each type of take-off and landing, as well as their execution methods.

2.6.1 Vertical take-off and landing

Vertical take-off and landing (VTOL) refers to a system in which support propellers are used to help the kite or wing take-off vertically until the energy production process begins. Various companies and research groups are studying this method. For instance, Makani, TwingTec, and KiteMill are some of the companies that focus on VTOL. TwinTec and KiteMill follow a similar approach that involves the kite or wing taking off vertically through the movement of propellers present in the prototype, similar to that of a helicopter. However, the main difference between them is the modifications and functionality that rotors can provide. KiteMill is able to offer more functionalities related to the specification that the propellers can do depending on the phase of flight it is in, a functionality that the TwingTec prototype cannot offer [21]. TwinTec has developed a patented solution that allows the kite or wing to fly smoothly while curved, compensating for the forces generated by the rotors [14]. In figures 2.9 and 2.10, we can see the prototypes of KiteMill and TwingTec respectively.



Figure 2.9: KiteMill prototype. (Source: [9])



Figure 2.10: TwingTec prototype. (Source: [10])

Makani uses a unique approach that sets it apart from the other models mentioned. Its rotors are situated on the top of the wing or kite, allowing for vertical take-off and landing, similar to a tailsitter aircraft [14]. In Figure 2.11, we can see the Makani Power prototype.



Figure 2.11: Makani prototype. (Source: [11])

This method of automatic take-off and landing provides the advantage of being able to take off and land in relatively small areas. However, the presence of rotors to assist the kite in taking off adds extra difficulty to control, as well as weight to the kite or wing, which is a disadvantage.

2.6.2 Linear or catapult take-off and landing

One of the methods used in horizontal take-off and landing is the linear or catapult take-off and landing. In this method, the prototype is accelerated horizontally until the necessary speed is reached to start flying and producing energy. An external energy source or an electromagnetic launch system is used to aid in this acceleration. Companies such as Ampyx Power and ElektRail have adopted this approach.

Ampyx Power is a company that has developed a unique system to generate energy. Their system uses a catapult to inject kinetic energy into the system during the launch phase, and a braking system that uses a rope to remove energy during landing. The design of this system is

specially made to minimize the area required to carry out the launch [22]. Ampyx Power is one of the few companies that have successfully developed a completely autonomous system that can execute all the flight phases from launch to energy production and landing [14]. In Figure 2.12, we can see the Ampyx Power prototype.



Figure 2.12: Ampyx Power prototype. (Source: [12])

ElektRail is a company that is developing a system that enables devices to take-off and land without the use of traditional landing gear [23]. This system offers several advantages, including reducing the weight of the device and the distance required for take-off, as the device is propelled by the system of the Earth. However, the landing process is highly complex and requires careful synchronization between the aircraft and the landing site. In the figure 2.13, we can see the ElektRail device.



Figure 2.13: ElektRail prototype. (Source: [13])

For this type of take-off and landing, a significant space is needed to perform both the launch and landing operations. In addition, extra equipment is required to assist with the initial acceleration. However, this method offers several benefits, particularly in terms of ensuring the stability of the device during the take-off and landing processes.

2.6.3 Circular take-off and landing

The circular take-off and landing method involves the kite gradually increasing its speed while making circular movements until it reaches the necessary height to produce energy, as mentioned in the study conducted by Gabriel Fernandes [14]. In figure 2.14, Antonello Cherubini introduced a model of a kite with an integrated motor that is controlled until it reaches the required speed for take-off [14].

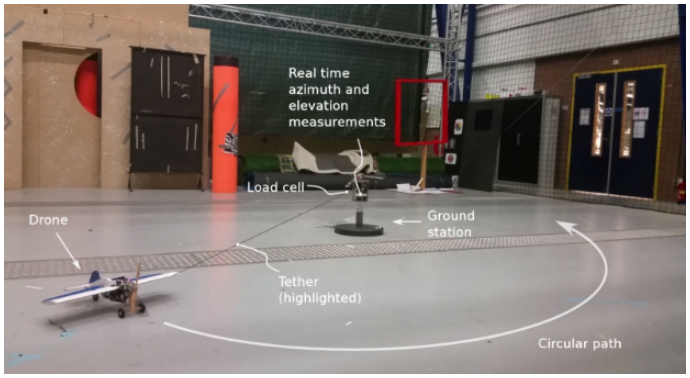


Figure 2.14: Fully automatic experimental circular take-off and landing. (Source: [14])

Out of all the approaches mentioned earlier, circular take-off and landing is the least commonly used method. Although it falls under the category of horizontal take-off and landing, it differs in terms of its characteristics, as illustrated in figure 2.6. EnerKite is one of the companies that has updated this type of take-off and landing. EnerKite employs a kite attached to a mechanical rotating arm, which rotates until it attains the required speed to enter the energy production phase. The prototype used by EnerKite is shown in the figure 2.15.



Figure 2.15: EnerKite prototype.(Source: [15])

This approach has some drawbacks in terms of the required area for take-off and landing, as well as the increased complexity of the system. However, it does not require any additional equipment for initial propulsion.

2.6.4 Comparison and Viability of Take-off and Landing Methods

In this section, we will compare three take-off and landing methods for airborne wind energy systems: vertical (VTOL), horizontal (HTOL), and circular (CTOL). Each method has its own advantages and disadvantages, which are crucial in determining their practicality for real-world applications.

2.6.4.1 Vertical Take-off and Landing (VTOL)

The vertical take-off and landing method offers a significant advantage in terms of space efficiency. It allows for take-off and landing in confined areas, making it particularly suitable for deployment in environments with limited space, such as urban or geographically restricted locations.

Nevertheless, this approach has some drawbacks, particularly due to the increased complexity and weight caused by the use of rotors or similar systems for take-off assistance. These additional components can impact the aerodynamic performance and energy efficiency of the kite or wing. Furthermore, the added control complexity required to manage the rotors makes the system more challenging to operate. Despite these disadvantages, the vertical method remains a viable solution in situations where space limitations are a primary concern, as its advantages in confined environments outweigh the drawbacks.

2.6.4.2 Horizontal Take-off and Landing (HTOL)

The horizontal take-off and landing method requires a larger operational area for both take-off and landing, limiting its applicability in space-constrained environments. This approach typically involves the use of additional equipment, such as catapults or rails, to provide the necessary acceleration for launching the kite.

On the positive side, horizontal take-off offers greater stability during the take-off and landing processes. However, the requirement for large open spaces and dependence on auxiliary equipment makes horizontal takeoff less practical for many real-world applications, especially in cases where installation space is limited.

2.6.4.3 Circular Take-off and Landing (CTOL)

The circular take-off and landing method has a unique advantage in that it does not require any additional propulsion equipment to initiate the take-off process. This absence of external systems results in a lighter and simpler overall setup, potentially reducing both operational costs and maintenance demands.

However, this method encounters the same space constraints as horizontal take-off and landing, necessitating a large area for take-off and landing. Additionally, the circular take-off introduces complexity to the control system when executing the circular trajectory to gain speed and height. Nevertheless, the reduced weight of the system and equipment requirements make it a highly feasible option in situations where ample space is available.

2.6.4.4 Viability Assessment

Considering the advantages and drawbacks of each method, the vertical and circular take-off methods emerge as the most viable options for practical implementation.

Vertical take-off and landing provides significant flexibility in space-limited environments. Its ability to operate in confined areas makes it well-suited for urban installations or regions with challenging topography. Despite the added weight and complexity of rotors, the benefits of operating in small areas make them a favorable solution in these particular situations.

Circular take-off and landing is unique because it does not require additional equipment for initial propulsion, making it a compelling choice in scenarios where larger operational areas are available. Although its control system is more sophisticated, the absence of external propulsion systems provides a distinct advantage.

The horizontal take-off and landing method provides greater stability but is less practical due to its reliance on large spaces and extra equipment. This limits its adaptability for widespread deployment. It may only be suitable for specific environments where space and resources are abundant, making it a less flexible option compared to the vertical and circular methods.

2.7 UPWIND Project

In this section, the prototype of the kite utilized in the UPWIND Project will be presented, accompanied by a comprehensive description of the forces acting upon it.

2.7.1 Prototype

In figures 2.16 and 2.17, we can observe the kite prototypes utilized in the UPWIND project for testing and simulations in a real environment.

When designing controllers for kite dynamics, it is crucial to analyze the forces acting on the kite. Regardless of the take-off method used, there are common and universal forces at play. In this thesis, the forces to be considered include the lift force (F_L), an auxiliary force denominated the push force (F_P) which will function as a propellant, the drag force (F_D), inertial forces (F_i), the gravitational force (F_g), and the tangential force (F_t).

The lift force is generated by the pressure difference between the top and bottom surfaces of the kite due to the wind flow. This force acts perpendicular to the wind direction and is crucial for keeping the kite in the air, maintaining altitude, and counteracting the gravitational force. It is a mechanical aerodynamic force produced by the motion of the airplane through the air [24, 25].

The push force in this system refers to an additional force that corresponds to the activation or deactivation of the kite motor. When the velocity of the kite is positive (when it is moving forward), the motor engages to provide thrust in the direction of motion. The primary purpose of this force is to assist in the acceleration of the kite during take-off or when extra propulsion is needed to overcome aerodynamic drag or gravity.

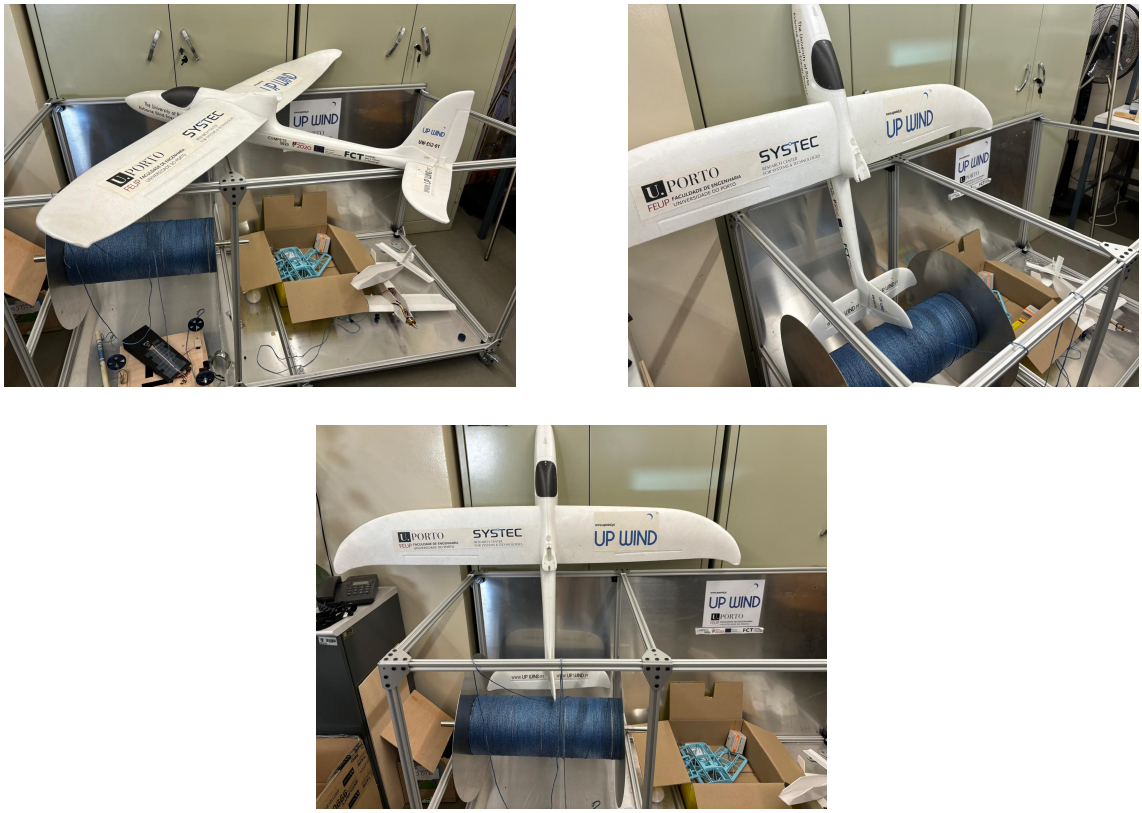


Figure 2.16: Prototype of the large kite.

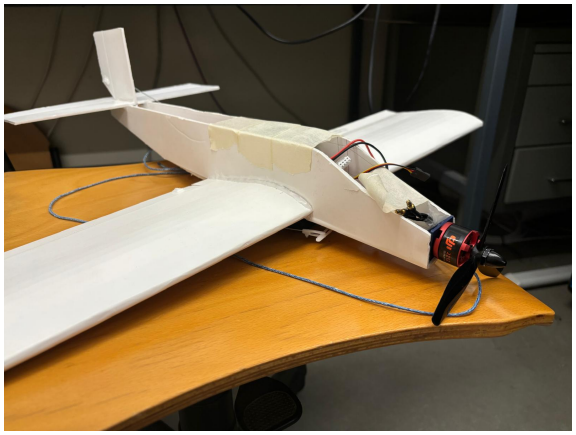


Figure 2.17: Prototype of the small kite.

Drag is the force that acts in the opposite direction to the wind and is caused by the resistance of the air as the kite moves through it. It serves to resist acceleration, so it is important to minimize drag to achieve optimal energy generation [26, 24].

Inertial forces are a set of forces that act on the kite and are associated with the acceleration and deceleration of the kite. These forces arise from changes in the speed or direction of the kite as it moves. They affect the stability and control of the kite and must be taken into account when discussing control maneuvers [27, 28].

The gravitational force is a force that acts downward due to the weight of the kite, which is influenced by the gravity of the Earth. This force pulls the kite downwards and needs to be counteracted in order to keep the kite in the air [29].

In conclusion, the tangential force is a force that, as the name suggests, acts alongside and tangents to the movement of the kite. This force is linked to the tension in the rope and the circular movement or take-offs that result from this tension. The tangential force significantly affects the trajectory and power generation cycle of the kite. This has been supported by [30, 25].

The combined effect of all forces on the kite determines its flight dynamics, stability, and efficiency in harnessing wind energy. Understanding these forces and their equilibrium is crucial for designing effective AWE systems.

2.7.2 Forces Diagram

When studying the motion of a pendulum, it is advantageous to create a visual representation in the form of a force diagram. This diagram provides a comprehensive illustration of the various forces acting on the pendulum and how they interrelate. It serves as a fundamental tool for translating these physical interactions into mathematical equations. These equations are pivotal for accurately defining the dynamic behavior of the pendulum and are essential for developing effective control strategies.

2.7.2.1 2D

In Figure 2.18, the diagram illustrates the coordinate system used to address the 2D level problem, which focuses on the x and z axes. Figure 2.18 (a) displays the coordinate system without the wind component, while (c) includes the wind direction aligned with the x-axis. The angles shown are the theta (θ) angle used to discuss pendulum motion, measured in relation to the z-axis in a positive counterclockwise direction, and the beta (β) angle, used in the UPWIND project for easier 3D-level problem calculations, representing the elevation angle ($\theta + \beta = 90º$). In our problem, it is measured in relation to the x-axis, moving in an anticlockwise direction. For clarity in diagramming, the kite is represented by a black circle in all diagrams and the center of mass by a blue circle in the force diagram. Figure 2.18 (b) shows the decomposition of forces acting on the kite and their respective directions. The local coordinate direction of the system is also illustrated, represented by the e_r and e_β axes, with e_ϕ omitted since only 2D considerations are relevant at this stage.

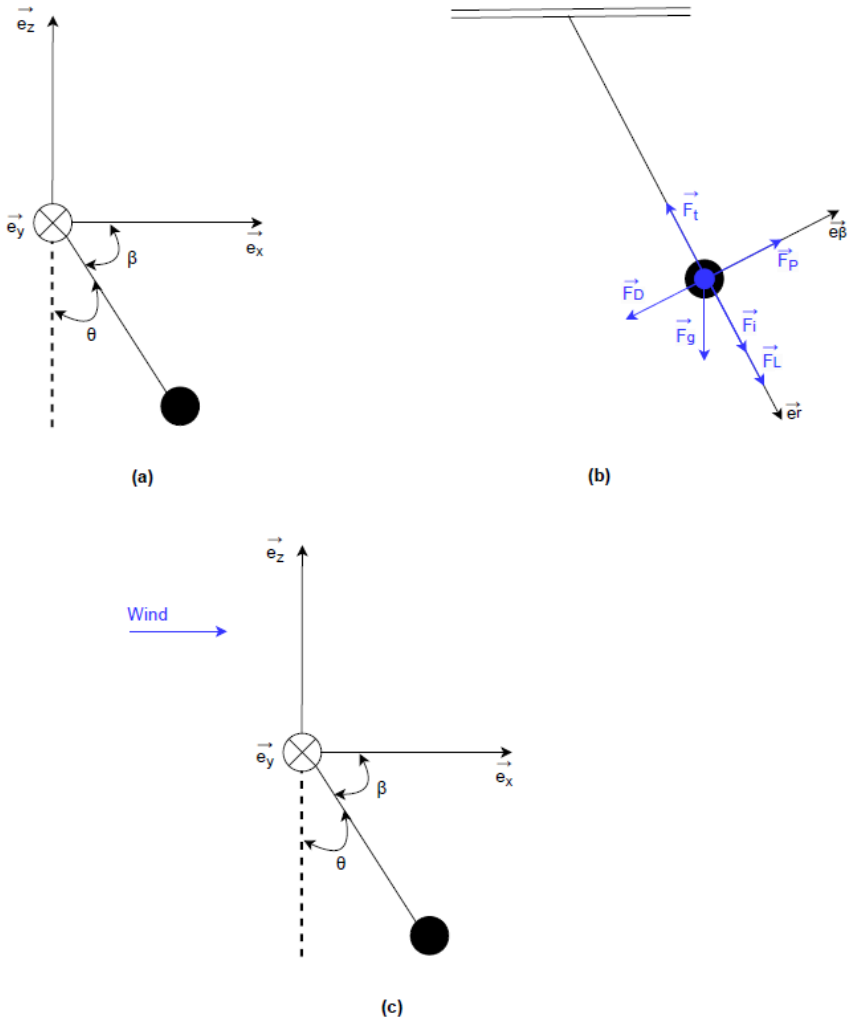


Figure 2.18: (a) The system coordinates for 2D are visible; (b) The forces diagram on the 2D kite is depicted; (c) The system coordinates and wind direction are shown for 2D purposes.

2.7.2.2 3D

When the problem is approached from a three-dimensional perspective, it is necessary to modify the coordinate system that is employed. It is thus necessary to project the various forces acting on the kite (see reference 2.7.1) onto the planes in order to facilitate the calculations and formalize the mathematical equations. The coordinate system relative to the body of the kite now plays an important role, as it is related to the aerodynamics of the kite and the realization of vertical, transverse, and horizontal movements. These movements are necessary for the kite to follow the defined trajectory. A more detailed explanation of this can be found in subsection 4.1.

Figure 2.19 illustrates the referential utilized in the three-dimensional problem, along with the orientation of its axes and pivotal angles, β and ϕ. These angles will be discussed in detail in the subsequent subsection, 4.1.

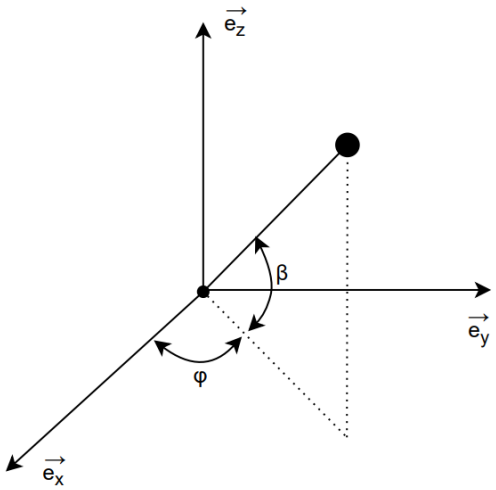


Figure 2.19: The system coordinates used for 3d simulation.

To simplify the mathematical formulations, a study was conducted by projecting the kite and its forces onto different planes. In the figure 2.20, the left side shows the side view of the kite, known as the lateral perspective. The projection onto the yz plane is oriented so that the x-axis points "out" of the plane, following the right-hand rule. The figure also illustrates the angle α, which represents the angle that the kite makes with the y-plane (the opening of the kite), and is set as a constant because we are considering a constant wind velocity. The parameter r indicates the length of the rope, while R represents the radius of the circumference. The circumference described by the kite is observed from a frontal perspective on the xz plane. The right of figure 2.20 illustrates the effect of wind velocity, resulting in an inclination of the kite and thus creating an opening angle. It also illustrates the circular trajectory of the kite from a front perspective, following the initial pendulum motion. It is crucial to note that in our 3D analysis, the wind is considered to be in the y-axis direction rather than the x-axis direction as previously discussed in 2.7.2.1. This slight variance means that as the kite moves, the wind will strike it perpendicularly, resulting in oscillations along the y-axis. The point where the wind hits the kite may also impact its trajectory, depending on whether it strikes the top or bottom of the kite.

In figure 2.21, we can observe the projection of the kite on the xz plane, which represents the front view of the trajectory of the kite. This trajectory is depicted as a circle. The orientations of the x and z axes are visible, as well as the direction of the y axis, which points "inside" the plane in accordance with the right-hand rule. It is important to note that the trajectory of the kite does not immediately form a complete circle as soon as it begins to move. Initially, the kite follows a pendulum motion that defines a half-circle. Once it reaches a sufficient velocity (denoted as $\vec{v}$) tangent to the trajectory, the kite then transitions to move in a circular trajectory. This shift indicates that the kite is ready to enter the energy production phase and engage the flight envelope. The flight envelope specifies the safe operational limits within which an aircraft can fly. These limits cover various parameters, including speed, altitude, load factor, and angle of attack. By

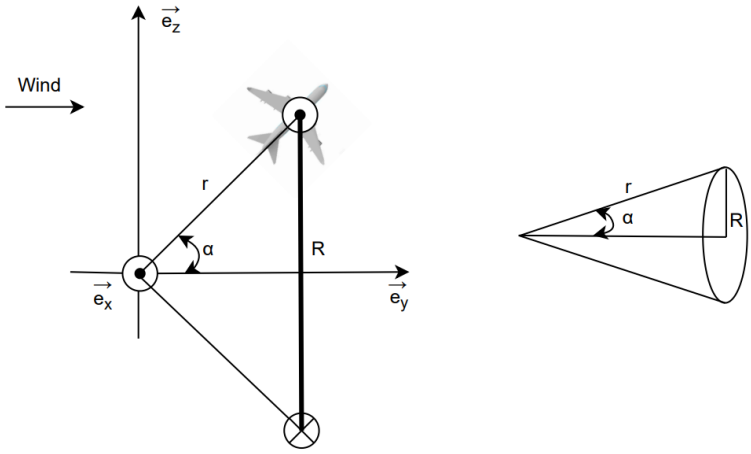


Figure 2.20: Visual representation of the kite in the yz plane. (Source: [16])

adhering to the flight envelope, the aircraft operates within safe boundaries, mitigating the risk of structural failure or loss of control [31, 32, 33, 34]. The figure also depicts the angle σ, which varies with the movement of the kite as it traces its trajectory. This angle is measured between the position of the kite and the x-axis and can range from 0 to $2\pi \times$n (0 to $360 \times$n), where n denotes the number of complete turns the kite will make before entering the production phase.

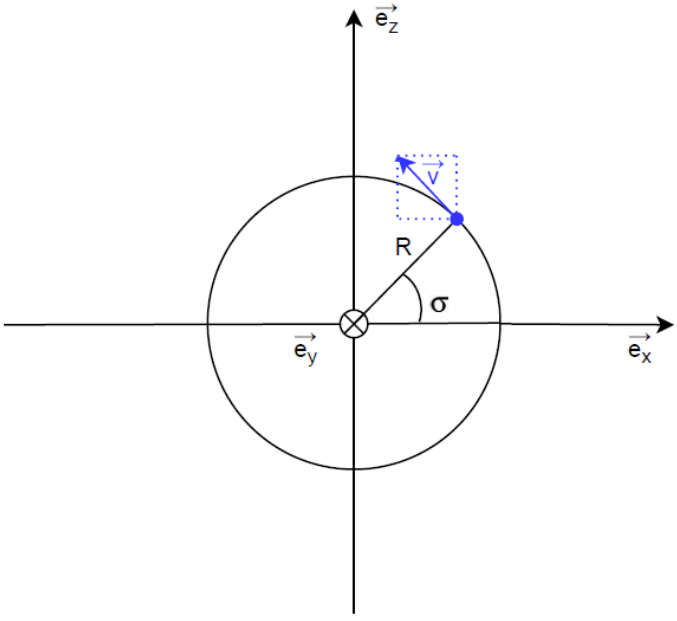


Figure 2.21: Visual representation of the kite in the xz plane and velocity vector.

Now that we have an overview of the coordinate systems and angles to be used for determining mathematical relationships, we can examine the decomposition of forces in more detail. In figure 2.22, we can see the decomposition and directions of the forces acting on the kite projected

onto the yz plane, from a lateral perspective. It is important to note that the drag force, F_D, and push force, F_P, act in the direction of the circular trajectory of the kite in the xz plane. The push force is directed "out" of the plane and the drag force is directed "into" the plane, following the right-hand rule. In this figure, we can also see the vector $\vec{e}_r$ representing the local coordinates, specifically in the radial direction, which will be further explained in the next sections.

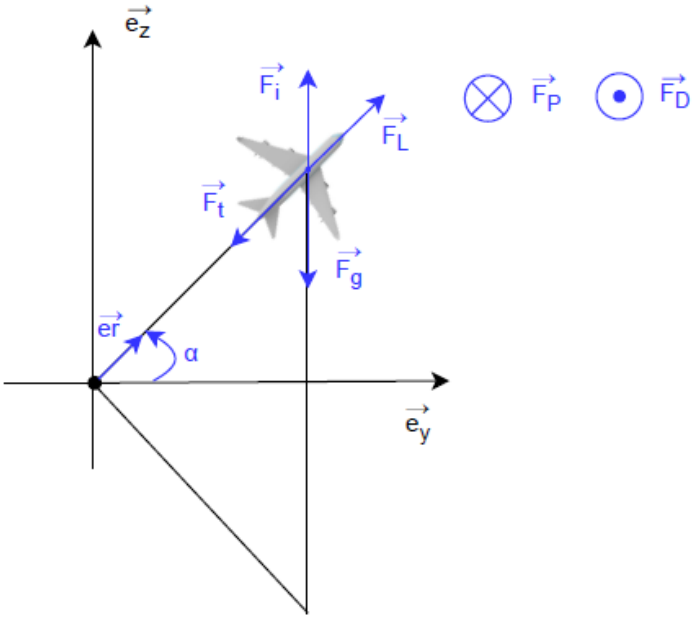


Figure 2.22: Visual representation of the forces acting on the kite in the plane yz. (Source: [16])

To better comprehend and visualize the drag, F_D, and push forces, F_P, and their orientations, we can project the forces onto the xz plane. This allows direct observation of their directions, where both forces are tangent to the trajectory but in opposite directions. We can also observe all the forces acting on the kite from a frontal perspective, their respective directions, and the angle σ that the kite makes with the x-axis. Figure 2.23 illustrates the projection of the forces onto the xz plane.

In figure 2.24, we can observe the body coordinates of the kite and their respective directions. These body coordinates are important for defining the direction of the lift force that will help the kite to ascend. A more detailed explanation of the body coordinates and the movements controlled by each vector $\vec{e}_{roll}$, $\vec{e}_{pitch}$, and $\vec{e}_{yaw}$ can be found in section 4.1. On the left-hand side of the figure, the arrangement of the body coordinates and the lift force, F_L can be seen in the yz plane, along with the roll angle, ϕ. The roll angle is the angle between the lift force F_L and the z-axis. It is the angle through which an airplane must be rotated about its longitudinal axis to bring its lateral axis into a horizontal plane. It is positive when the left wing is higher than the right [35].

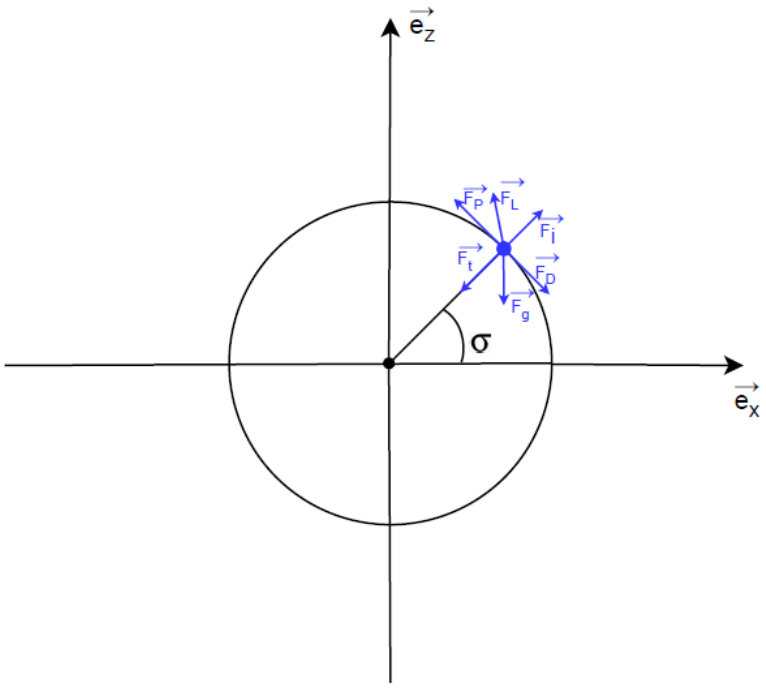


Figure 2.23: Visual representation of the forces on the plane xz.

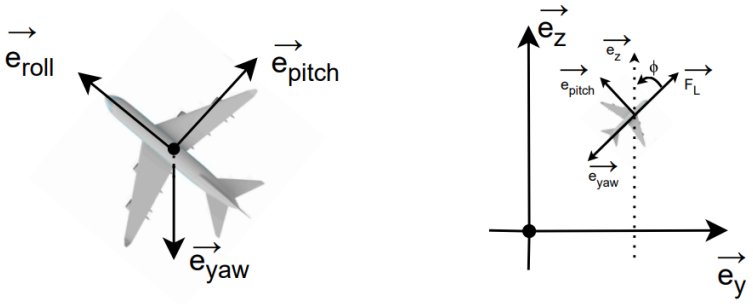


Figure 2.24: Kite Body coordinates (left); Body coordinates diagram representation (right). (Source: [16])

Chapter 3

Simple Pendulum System

3.1 Preliminary Work

This section will expound on the most pertinent theoretical aspects related to the thesis topic. Specifically, it will focus on providing an overview of the current state of the art and introductory work. Furthermore, this section will delve into more detailed research on the topic and the creation of introductory simulations using Matlab. The primary objective of these simulations is to evaluate initial concepts for the project and to gain familiarity with the features of the Matlab simulation software.

3.1.1 Problem Description

In this section, we will briefly explain the problem and provide some equations that will serve as the basis for initial testing and simulations. This thesis aims to develop an automatic controller that uses a pendulum approach for take-off. The pendulum approach will take into account a wide range of forces that will be acting on the kite, including drag (F_D), push (F_P), lift (F_L), inertial (F_i), gravitational (F_g), and tangential forces (F_t). The pushing force will only exist in the positive direction of the speed, which means there will be no pushing force when the speed is negative. This is similar to a swing being pushed. The person pushing the swing corresponds to activating the motor (the push force), which gives the swing an impulse to move forward and then backward. There is no impulse when the swing moves backward, only when it moves forward. This is an analogy of what will happen with the kite. The kite will swing back and forth, until it reaches enough speed. Once the kite reaches its maximum speed and follows a circular trajectory, we will know that it is ready to take-off.

To achieve the objective of the project, we conducted simulations and research to simulate the pendulum movement of a body with a mass of 1 kg and later on with a mass of m kg. The diagram in Figure 3.1 illustrates the forces acting on a simple pendulum - the tension in the rope with length L and the gravitational force - during its trajectory.

When discussing pendulum motion, the most important variable to consider is the angle, represented by theta (θ). However, in the UPWIND project, the angle of interest is not theta (θ) but

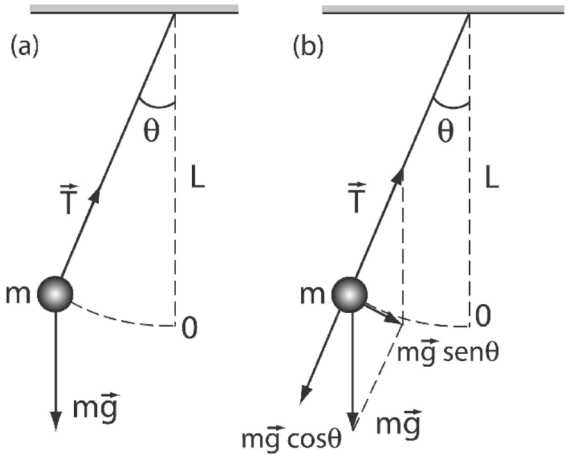


Figure 3.1: Simple pendulum - initial position (a) and forces acting on the body of mass during its trajectory (b). (Source: [17])

beta (β), which is equal to 90 degrees minus theta (90º-θ). In this particular test, we are focusing on the theta angle. If we were to utilize the angle β as in the UPWIND project, we would use sin(90-θ) which is equivalent to sin(β).

We only used 2D simulations, using the x and z axes and assuming that there are no forces acting perpendicular to the plane. The code was developed using formulas 3.1 and 3.2 [36, 37, 38].

$$\frac{d^2\theta}{dt^2} = -\frac{g}{L} \cdot \sin(\theta); \tag{3.1}$$

$$\frac{d^2\theta}{dt^2} = -\frac{m \cdot g}{L} \cdot \sin(\theta); \tag{3.2}$$

In these formulas, θ represents the angle with the vertical, L represents the length of the cable, m represents the mass in kilograms (kg), and g represents the gravitational acceleration, which is considered to be 9.81 m/s^2. The expression $\frac{d^2\theta}{dt^2}$ represents angular acceleration.

To develop the code, we initially established the parameters and subsequently utilized the ODE function to solve the equations referenced as 3.1 and 3.2. A more detailed explanation of the ODE function will be provided in the 2D implementation of the kite 4.2.1.1.

3.1.2 Results and Discussion

The application of the formulas referenced in 3.1 and 3.2 facilitated the generation of diverse graphs, enabling a more rigorous analysis of the trajectory and the θ angle. Additionally, an animated representation was utilized to observe the movement of the pendulum over time.

In the initial phase, simulations were executed utilizing the formula denoted in 3.1. In the animation shown in 3.2, the temporal motion of the pendulum is analyzed. It exhibits a consistent

variation in the angle θ, ranging from $\frac{\pi}{2}$ to -$\frac{\pi}{2}$ radians, equivalent to 90º and -90º, respectively. Notably, when the pendulum is at the origin, it reaches a 0º position, signifying vertical elongation.

In Figure 3.3, we can observe the trajectory described by the pendulum without interference from external variables. The pendulum starts at the position of 90º ($\frac{\pi}{2}$ radians), represented by a red circle in the figure (3.3), and moves for a defined time of 10 seconds. After these 10 seconds, the pendulum ends up in a given position, represented by the green circles in Figure 3.3.

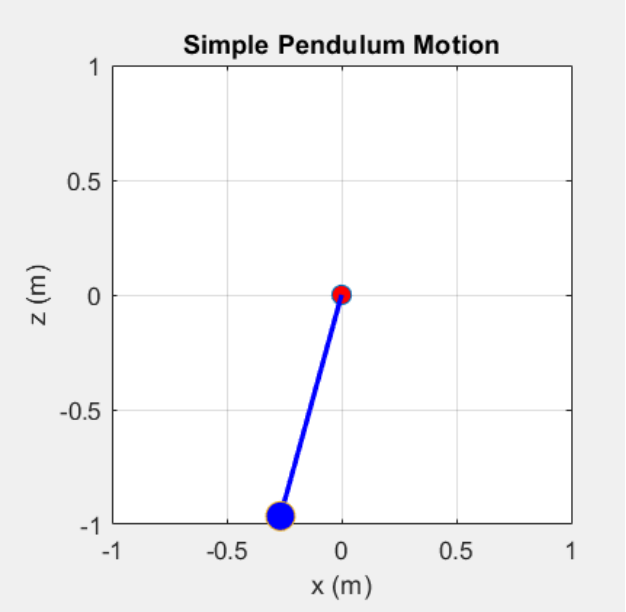


Figure 3.2: Animation of the pendulum motion for mass 1kg.

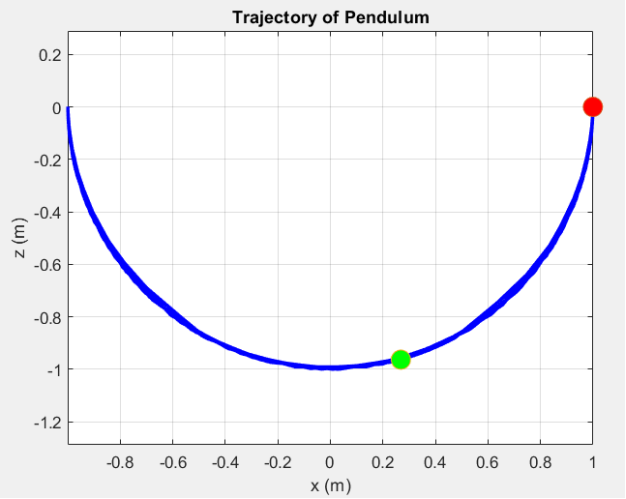


Figure 3.3: The trajectory of the motion of the pendulum for mass 1kg.

In the context of figure 3.4, we can observe the angle θ changing over time. The trajectory of the pendulum begins at approximately 89.9281º when t = 0 seconds. As the pendulum moves from $\frac{\pi}{2}$ to -$\frac{\pi}{2}$ radians (90º to -90º), the graph is in the upper part of the angle θ-axis, representing a

positive direction of movement. Conversely, when the pendulum moves from -$\frac{\pi}{2}$ to $\frac{\pi}{2}$ radians (-90º to 90º), the θ is negative, indicating movement in the opposite direction. Whenever the pendulum reaches the 0º position, the graph crosses the origin. As we can see, the graph accurately depicts the expected trajectory and movement through animation.

When observing the graphs of the angle θ, we see that the angle varies consistently, with a constant amplitude and period. This is because there are no external forces, such as a push force or drag force, to alter the movement. Since only the weight and tension are acting on the system, the variation remains uniform.

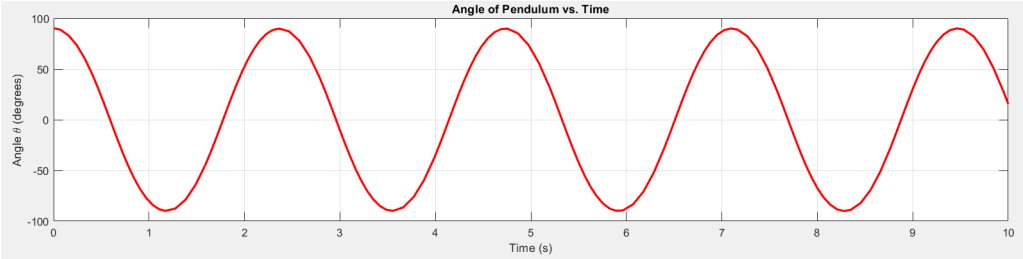


Figure 3.4: Graphic of the variation of the angle θ through time for mass 1kg.

When employing the formula 3.2, which accommodates a mass value other than 1 kg (in this case, 2 kg), our observations show that the behavior of the pendulum closely resembles that of a pendulum with a 1 kg mass. The figures 3.5 and 3.6 show the motion of the pendulum and trajectory over a 10-second interval. Compared to the graph of the 1 kg pendulum, the trajectory, and simulation are practically the same. Observing the effects of the introduction of the variable m in the equation, we can conclude that there is practically no impact on the trajectory and motion.

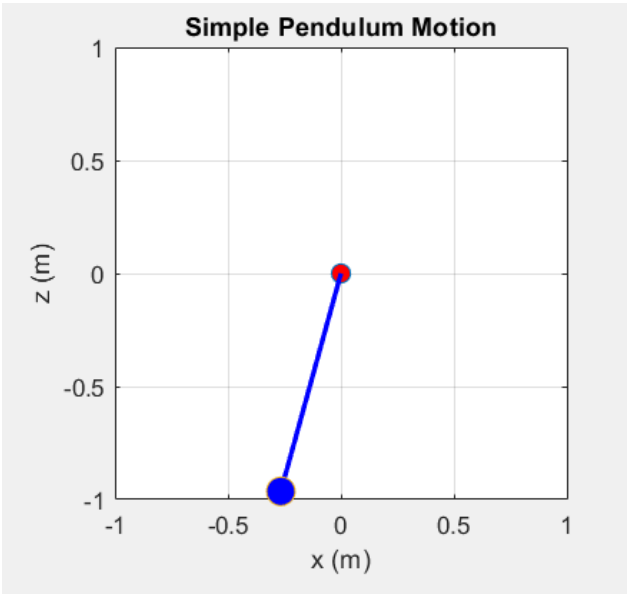


Figure 3.5: Animation of the pendulum motion for mass m kg.

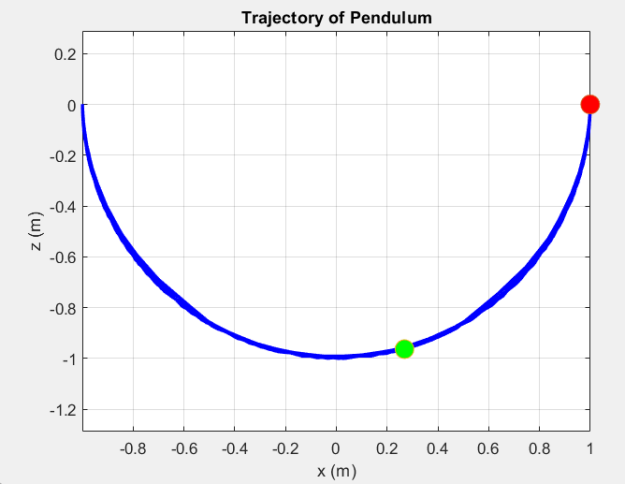


Figure 3.6: The trajectory of the motion of the pendulum for mass m kg.

In the θ graph (figure 3.7), we notice some differences compared to the graph with a mass of 1kg (figure 3.4). The behavior is similar to the 1 kg mass graph when moving in the positive direction from $\frac{\pi}{2}$ to -$\frac{\pi}{2}$ radians (90º to -90º); θ is positive and at the upper part of the angle θ-axis. When moving in the negative direction from -$\frac{\pi}{2}$ to $\frac{\pi}{2}$ radians (-90º to 90º), θ is at the bottom of the graph. The position at t = 0 seconds is different, starting at a value of approximately 89.7122º instead of 89.9281° as seen previously (3.4).

This difference is related to the inclusion of the variable *m* in the formula (equation 3.2), which was not considered in equation 3.1. Therefore, when adding a variable that was not previously present and directly influences the formula, the values are expected to be slightly different despite having similar behaviors, and we can see the impact on the values.

When comparing a kite with a mass of 2 kg to one with a mass of 1 kg, the value of the angle θ at t = 0 seconds is $\frac{89.7122}{89.9281} \approx 0.9976$. When we double the mass, the value of the angle θ decreases by 0.9976. In conclusion, by observing the difference at t = 0 seconds, we can see the impact of adding the variable *m* in the equation in terms of the values of the angle θ. Additionally, we can once again conclude that the angle variation remains constant, as previously explained, due to the absence of external forces causing variations in the system.

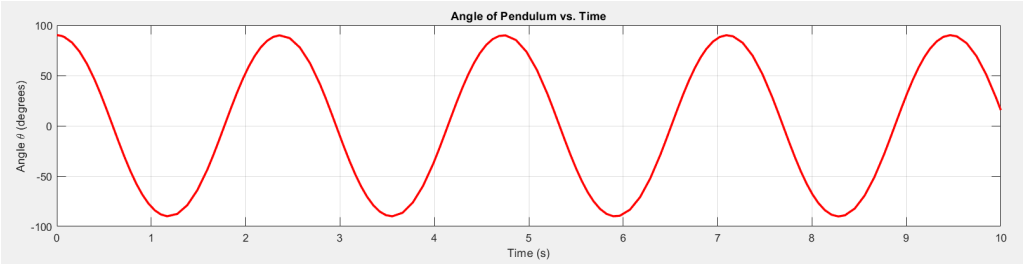


Figure 3.7: Graphic of the variation of the angle θ through time for mass m kg.

After using specific formulas and analyzing the results, we gained a better understanding of

how pendulum movement functions. This understanding is a fundamental concept that will be applied in the development of the kite take-off controller. Additionally, these simulations helped us become familiar with the Matlab simulation software and its tools. Based on the applied formulas and subsequent analysis, we have gained a comprehensive understanding of pendulum movement, a foundational concept essential for the development of the kite take-off controller. These simulations have also facilitated our proficiency with the Matlab simulation software and its associated tools.

Chapter 4

Kite Model

4.1 Coordinate System

Studying and analyzing the physical model of an Airborne Wind Energy System (AWES) is a crucial step in ensuring that its autonomous actions and movements can be controlled and predicted effectively, resulting in optimal performance [14]. The UPWIND project has chosen to use a simulation model based on a mass point that operates using three coordinate systems: global (G), local (L), and body (B). This model greatly simplifies the simulation process and enables accurate prediction of the trajectory of the kite [14].

The global coordinate system (G) is a Cartesian inertial coordinate system that is characterized by three vectors ($\vec{e}_x$, $\vec{e}_y$, $\vec{e}_z$). The origin of this system represents the location where the cable is fixed, as mentioned in [14, 39]. To simplify the model, the wind speed is assumed to be in the same direction as the x-axis ($\vec{e}_x$).

The local coordinate system (L) is a non-inertial spherical coordinate system that is defined by three vectors ($\vec{e}_r$, $\vec{e}_\phi$, $\vec{e}_\beta$). We use spherical coordinates to make calculations easier. To get the position of the kite in the global coordinate system (G), we need to transform the spherical coordinates into Cartesian coordinates. In this transformation, we do not use the angle β shown in figure 4.1.

Instead, we use the angle 90°-β corresponding to the β angle in figure 4.2. This is because it makes more sense to consider the ascent angle. When we do the transformations from spherical to Cartesian coordinates, this small change means that we need to swap $\sin(\beta)$ for $\cos(\beta)$ and $\cos(\beta)$ for $\sin(\beta)$ in the traditional transformation.

The body coordinate systems (B) are defined by the vectors ($\vec{e}_1$, $\vec{e}_2$, $\vec{e}_3$), which correspond to the body of the kite. These vectors control specific parts of the movement of the kite, with $\vec{e}_1$ controlling longitudinal movement, $\vec{e}_2$ controlling transverse movement, and $\vec{e}_3$ controlling vertical movement. These movements correspond respectively to the roll, pitch, and yaw movements [14, 39]. The origin of the body coordinate system corresponds to the center of mass of the kite itself [14, 39], as shown in figure 4.3.

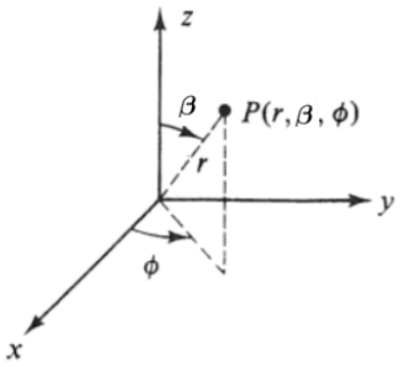


Figure 4.1: Global and Local coordinate systems.

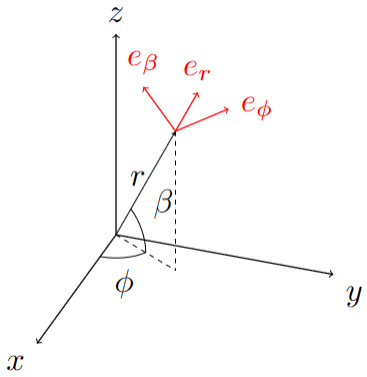


Figure 4.2: Global and Local coordinate systems used in UPWIND. (Source: [14])

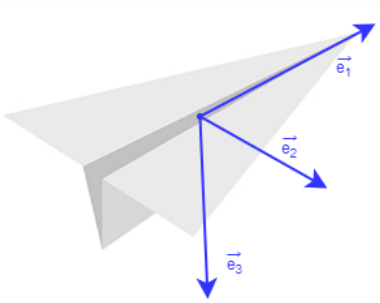


Figure 4.3: Body Coordinate Systems. (Source: [18])

As mentioned earlier, the vector $\vec{e_1}$ denotes the longitudinal direction of movement and is in line with the direction of travel of the kite. The vector $\vec{e_2}$ governs lateral movement and is situated on the right wing of the kite. Finally, the vector $\vec{e_3}$ controls vertical movement from top to bottom. These vectors play a crucial role in directing the movements of the kite, as previously explained. Their functionality is vital for guiding the kite along its flight path, from take-off to landing.

4.2 Kite Model

4.2.1 2D Dimensions

Before we start working on 3D analysis, which involves consideration of the y-axis, we will first concentrate on 2D analysis. Initially, the wind force v_w was not considered, but later we included its effect in the x-axis direction.

Initially, we decomposed the forces to analyze the various forces acting on the kite, as outlined in Section 2.7.1 and illustrated in Figure 4.4. This force analysis enables us to determine the global coordinates required for subsequent calculations and simulations.

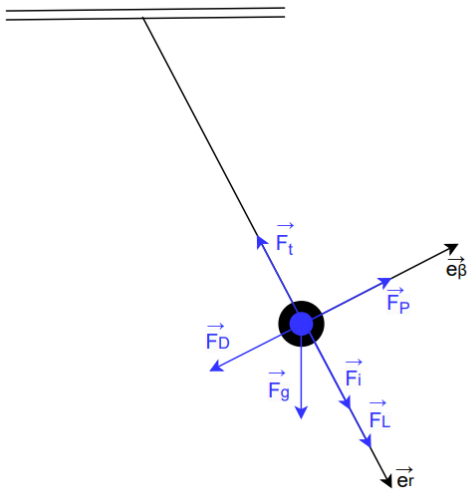


Figure 4.4: Forces Diagram.

It is important to consider the chosen coordinate system and axes when decomposing forces. For 2D analysis, it is crucial to establish the specific axes being used. In this case, we are focusing on the x and z axes, assuming that the kite stays still along the y-axis. For a more detailed explanation, you can refer to the previously discussed sub subsection 2.7.2.

To analyze the forces acting on the kite, we begin by examining the global coordinates using a system of axes and the breakdown of forces. Initially, we utilize the angle θ, which is commonly employed in calculations. Then, we convert it to the angle used in the UPWIND project, which is represented as β and can be obtained by taking 90 degrees minus θ (90º-θ).

In section 4.1, we discuss the use of angle β because it is important to consider the elevation angle of the kite. This angle represents the angle between the kite and the xy plane. Understanding this angle is crucial for knowing how the kite is positioned relative to the ground and how it might impact the performance and trajectory of the kite in Airborne Wind Energy Systems. It is important to note that this angle is different from angle θ, which represents the angle between the kite and the z-axis. Angle θ is more commonly used in the context of Airborne Wind Energy to describe the

orientation of the kite in the vertical plane. Analyzing the forces acting on the kite and optimizing its performance often relies on understanding this angle.

By decomposing the forces, we can derive the formulas that describe the forces acting on the kite in relation to the angle θ with the z-axis. These forces are represented by the equations in (4.1), (4.2), (4.4), (4.5), and (4.6).

$$\vec{F_g} = -m \cdot g \tag{4.1}$$

$$\vec{F_D} = -F_D \cdot cos(\theta) \cdot \vec{e_x} - F_D \cdot \sin(\theta) \cdot \vec{e_z} \tag{4.2}$$

$$\vec{F_L} = F_L \cdot \sin(\theta) \cdot \vec{e_x} - F_L \cdot \cos(\theta) \cdot \vec{e_z} \tag{4.3}$$

$$\vec{F_P} = F_P \cdot \cos(\theta) \cdot \vec{e_x} + F_P \cdot \sin(\theta) \cdot \vec{e_z} \tag{4.4}$$

$$\vec{F_i} = F_i \cdot \sin(\theta) \cdot \vec{e_x} - F_i \cdot \cos(\theta) \cdot \vec{e_z} \tag{4.5}$$

$$\vec{F_t} = -F_t \cdot \sin(\theta) \cdot \vec{e_x} + F_t \cdot \cos(\theta) \cdot \vec{e_z} \tag{4.6}$$

When we apply the transformation 90º-θ to the previous formulas, we can obtain the formulas for angle β. Angle β is the desired angle used in calculations and simulations. Equations 4.7, 4.8, 4.9, 4.10, 4.11, and 4.12 are similar to the previous equations and represent the decomposition of forces, but for the angle β.

$$\vec{F_g} = -m \cdot g \tag{4.7}$$

$$\vec{F_D} = -F_D \cdot \sin(\beta) \cdot \vec{e_x} - F_D \cdot \cos(\beta) \cdot \vec{e_z} \tag{4.8}$$

$$\vec{F_L} = F_L \cdot \cos(\beta) \cdot \vec{e_x} - F_L \cdot \sin(\beta) \cdot \vec{e_z} \tag{4.9}$$

$$\vec{F_P} = F_P \cdot \sin(\beta) \cdot \vec{e_x} + F_P \cdot \cos(\beta) \cdot \vec{e_z} \tag{4.10}$$

$$\vec{F_i} = F_i \cdot \cos(\beta) \cdot \vec{e_x} - F_i \cdot \sin(\beta) \cdot \vec{e_z} \tag{4.11}$$

$$\vec{F_t} = -F_t \cdot \cos(\beta) \cdot \vec{e_x} + F_t \cdot \sin(\beta) \cdot \vec{e_z} \tag{4.12}$$

In equations 4.1 and 4.7, the gravitational force, $\vec{F_g}$, remains constant regardless of the angle. This consistency arises from the fact that the gravitational force is angle-independent. When dealing with kite parameters in equations, we introduce several variables such as m for mass, g for gravitational acceleration (9.81 m/s^2), and F_g, F_D, F_L, F_P, F_i, and F_t, which represent the magnitudes of the forces. Additionally, we denote the directions of the x and z axes using $\vec{e_x}$ and $\vec{e_z}$, respectively.

Once we have obtained the global coordinates, we can proceed to derive the local coordinates. Using local coordinates facilitates the practicality of conducting tests and simulations. To convert global coordinates into local coordinates, we can employ the formula specified in Equation 4.13.

$$\begin{bmatrix} e_\beta \\ e_r \end{bmatrix} = \begin{bmatrix} \sin(\beta) & \cos(\beta) \\ \cos(\beta) & -\sin(\beta) \end{bmatrix} \begin{bmatrix} e_x \\ e_z \end{bmatrix} \tag{4.13}$$

By applying the conversion matrix from the global to the local coordinate system, as shown in Equation 4.13, the previously derived equations 4.7, 4.8, 4.9, 4.10, 4.11, and 4.12 can be transformed to represent the forces in the local coordinate system. The resulting equations 4.14, 4.15, 4.16, 4.17, 4.18, and 4.19 provide a more convenient and intuitive representation of the forces acting on the system in the local frame of reference.

$$\vec{F_g} = m \cdot g \cdot \sin(\beta) \cdot \vec{e_r} - m \cdot g \cdot \cos(\beta) \cdot \vec{e_\beta} \tag{4.14}$$

$$\vec{F_P} = F_P \cdot \vec{e_\beta} \tag{4.15}$$

$$\vec{F_D} = -F_D \cdot \vec{e_\beta} \tag{4.16}$$

$$\vec{F_L} = F_L \cdot \vec{e_r} \tag{4.17}$$

$$\vec{F_i} = F_i \cdot \vec{e_r} \tag{4.18}$$

$$\vec{F_t} = -F_t \cdot \vec{e_r} \tag{4.19}$$

With the forces already defined according to the local coordinate system, we are able to combine these forces while taking into account their respective directions. This encompasses the radial direction, e_r, the angular direction, e_β, or both, as observed in the case of the gravitational force, F_g.

In the radial direction (e_r), we have:

$$F_i + F_L - F_t + m \cdot g \cdot \sin(\beta) = 0 \tag{4.20}$$

And in the angular direction (e_β), we have:

$$F_P - F_D - m \cdot g \cdot \cos(\beta) = m \cdot \ddot{\beta} \tag{4.21}$$

These equations describe the forces acting on a kite in an airborne wind energy system in both radial and angular directions.

In the equation 4.20, we notice that the sum of forces in the radial direction e_r equals 0. In order for the kite to maintain equilibrium or experience steady-state motion in the radial direction, the collective sum of forces in the radial direction must be zero. Therefore, for simplicity, we assume that there is no movement in the radial direction and only consider movement in the angular direction. The sum of forces in the angular direction is equal to $m \cdot \ddot{\beta}$, following Newton's Second Law, where $\ddot{\beta}$ represents the acceleration. Newton's Second Law of Motion states that the total force acting on an object is equal to the mass of the object multiplied by its acceleration. In formulaic terms, this is expressed as $F_{total} = m \cdot a$.

The control parameters are determined by the sum of forces in the angular direction e_β, as already explained. When we equate the sum of forces in the angular direction, we get an equation involving the mass multiplied by $\ddot{\beta}$, as already described. Since $\ddot{\beta}$ represents acceleration and $\dot{\beta}$ represents velocity, we use these variables to determine when to activate the push force F_P by observing the direction of $\dot{\beta}$. We can do this by using the system of equations related to β and w.

To create the P-type controller, we use a system of equations involving the parameters β and w, as previously stated. Equation 4.22 shows the system of equations used to determine the desired speed.

$$\begin{cases} \dot{\beta} = w \\ \dot{w} = \ddot{\beta} = \frac{1}{m} \cdot (F_P - F_D - m \cdot g \cdot \cos(\beta) \end{cases} \tag{4.22}$$

With the system of equations that defines the controller, we can calculate the velocity, denoted as $\dot{\beta} = w$, and its corresponding direction. The magnitude of the velocity is determined by the result obtained from the acceleration equation, given by $\dot{w} = \ddot{\beta} = \frac{1}{m} \cdot (F_P - F_D - m \cdot g \cdot \cos(\beta))$. Integrating the acceleration equation allows us to determine the velocity, which is further elaborated in equation 4.23.

$$w = \dot{\beta} = v_0 + \dot{w} \cdot t \tag{4.23}$$

When deciding whether to engage the push force, F_P, it is essential to consider the direction of the speed - whether it is positive or negative. The push force is responsible for initiating movement by engaging the motor. We activate the push force when the speed is positive and disable it when it is negative. This alternating activation and deactivation creates a swinging movement reminiscent of a pendulum. In Equation 4.24, we have a system that serves as a switch to control the push force, F_P, based on the speed. If w > 0, then F_P is 1 (arbitrary); if w <= 0, it is 0. At w = 0, we cannot apply the push force, as it may hinder movement, particularly at extreme positions, such as -90º or 90º ($\frac{\pi}{2}$ or -$\frac{\pi}{2}$ radians), where ambiguity regarding activation of the force may lead to blocked or interrupted movement.

$$F_P = \begin{cases} 1 & \text{if } w > 0 \\ 0 & \text{if } w \leq 0 \end{cases} \tag{4.24}$$

In contrast to the push force, F_P, which has an arbitrary magnitude of 1 Newton as assigned earlier (see equation 4.24), the drag force, F_D, has a specific formula that depends on certain parameters to determine its magnitude. In equation 4.25, the calculation of the drag force involves replacing the parameters v_a, ρ, A, and C_D with the specific values used and defined within the scope of the UPWIND project. The parameter v_a represents the apparent wind speed in m/s, A represents the kite area in m^2, C_D represents the drag coefficient, and ρ represents the air density in kg/m^3.

$$F_D = \frac{1}{2} \cdot \rho \cdot A \cdot C_D \cdot v_a^2 \tag{4.25}$$

The lift force, F_L, is currently not a consideration in the 2D scenario, as it only appears in the e_r equation where the combined forces equal 0 to maintain equilibrium. However, it does possess a specific magnitude and is determined by the formula outlined in equation 4.26. The parameters used to calculate the lift force, F_L, are the same as those used for the drag force, F_D, with identical values, except for the inclusion of the lift coefficient, C_L, instead of the drag coefficient, C_D. Similar to C_D, C_L also has specific and defined values within the scope of the UPWIND project.

$$F_L = \frac{1}{2} \cdot \rho \cdot A \cdot C_L \cdot v_a^2 \tag{4.26}$$

In our implementation, we assumed that when there is no wind, the apparent wind speed (v_a) equals the kite velocity as calculated in equation 4.23. This allowed us to use the formula in equation 4.29, with the wind speed (v_w) set to 0. Therefore, v_a = w - 0, simplifying to v_a = w. This represents the kite velocity obtained using the formula explained in equation 4.27.

$$v_a = w = \dot{\beta} = v_0 + \dot{w} \cdot t \tag{4.27}$$

In the equation used to calculate drag force, denoted as F_D, if we neglect the effect of the wind, we can simply substitute the drag force (F_D) with the formula referenced in 4.28. Because there is no wind speed, the apparent speed is equal to the velocity of the kite w.

$$F_D = \frac{1}{2} \cdot \rho \cdot A \cdot C_D \cdot v_a^2 = \frac{1}{2} \cdot \rho \cdot A \cdot C_D \cdot w^2 \tag{4.28}$$

When taking into account the wind speed, v_w, which has a predefined value of 5 m/s, some slight modifications are needed for the previously mentioned formulas. Instead of the assumption mentioned and observed in Equation 4.27, we now need to consider the wind speed in the calculations of apparent speed. To calculate the apparent speed, we must find the difference between the speed obtained in the calculations (Equation 4.23) and the assigned wind speed (Equation 4.29).

This adjustment is necessary because, in this scenario, the influence of the wind affects the calculations, where the apparent speed is the vector between the velocity of the kite and the actual wind speed.

$$v_a = v - v_w = w - v_w \tag{4.29}$$

This slight adjustment in the velocity calculation will directly affect the calculation of the drag force, F_D. Instead of setting v_a equal to w, we will replace v_a with the apparent difference in 4.29, as shown in 4.30.

$$F_D = \frac{1}{2} \cdot \rho \cdot A \cdot C_D \cdot v_a^2 = \frac{1}{2} \cdot \rho \cdot A \cdot C_D \cdot (v - v_w)^2 = \frac{1}{2} \cdot \rho \cdot A \cdot C_D \cdot (w - v_w)^2 \tag{4.30}$$

We have made a small modification to the drag force, F_D, by introducing wind as a variable in our analysis. This has led to the development of a drag equation, which is dependent on the wind variable aligned with the x-axis. Considering the impact of wind on the equations and systems of equations mentioned in equation reference 4.22, along with the speed, has allowed us to conduct a more realistic analysis considering real-time factors such as the wind.

It is important to note that by integrating the velocity, we can also find the position x of the kite along the trajectory using the equations of motion given by the formula shown in 4.31.

$$x = x_0 + v_0 \cdot t + \frac{1}{2} \cdot \dot{w} \cdot t^2 \tag{4.31}$$

Where $\dot{w}$ represents the acceleration, x_0 the initial position, and v_0 the initial velocity.

4.2.1.1 Implementation

To simplify the process, MatLab was employed to conduct simulations and generate graphs based on the obtained results.

The code implementation involves initially defining the parameters using real data provided by the UPWIND group. The data presented in the simulations ranges from 4.32 to 4.40. Angles are measured in radians.

$$\rho = 1.223\,\text{kg/m}^3 \tag{4.32}$$
$$A = 0.7\,\text{m}^2 \tag{4.33}$$
$$m = 0.4\,\text{kg} \tag{4.34}$$
$$C_D = 0.05 \tag{4.35}$$
$$C_L = [1.7, 2.4] \tag{4.36}$$
$$L = 1.3\,\text{m} \tag{4.37}$$
$$g = 9.81\,\text{m/s}^2 \tag{4.38}$$
$$\beta_0 = -\frac{\pi}{2} \tag{4.39}$$
$$v_0 = 0.001\,\text{m/s} \tag{4.40}$$

Once the parameters had been defined, we proceeded to define the calculation of forces in local coordinates. The magnitude value of 1 Newton was assigned to the force F_P, as seen, in 4.10 and the drag force, F_D, was defined, taking into account the equation presented previously in 4.25. The magnitudes of F_i and F_t were also defined, although they were not used for calculations and simulations. The variables β and the speed w are the variables of interest and vary over time. As they are variables on which the forces are dependent in the code, when carrying out the calculation using the formulas located above, we place @(a,b) with the set of variables a or b on which the calculated forces are dependent, namely w and β. The syntax used was presented in 4.41 and 4.42.

$$F_D = @(\mathrm{w}, \beta) \text{ Equation } 4.25 \tag{4.41}$$

$$F_P = @(\mathrm{w}) \text{ Equation } 4.10 \tag{4.42}$$

In order to solve the system of equations outlined in 4.22 that define the kite controller and determine its speed, we utilized an ordinary differential equation (ODE). This allowed us to input the desired parameters and obtain corresponding outputs over a period of time (t measured in seconds), resulting in a set of solutions with one or more columns (y).

The ODE, or "ordinary differential equation," is a mathematical model designed to solve differential equations, initial value problems, and various properties. These solvers can handle rigid or non-rigid problems, mass matrix problems, differential algebraic equations (DAEs), or fully implicit problems [40].

In order to clarify the syntax and operation of the ODE, we will use an example from the reference [40] to illustrate the functioning of the ODE and the application of our observations to our specific problem of solving the condition system of the controller for our kite 4.22.

We are considering a first-order system of the type presented in the reference 4.43.

$$\begin{cases} y'1 = y2 \\ y'2 = y1y2 - 1 \end{cases} \tag{4.43}$$

In accordance with the system illustrated in equation 4.43, when employing the differential equation (ODE) approach, the code to solve the system of equations will be analogous to or equivalent to that demonstrated in the function 4.1.

```
function dy = ODE(t,y)
    dy(1) = y(2);
    dy(2) = y(1)*y(2)-2;
end
```

Function 4.1: ODE Function on MATLAB

After applying the ODE to the system of equations that define the controller, we defined the time interval in which the simulation would run and the initial conditions, which will be the values

that will be used and placed in ode45. ODE45 will solve the ODE, taking into account the defined time interval. In this case, we utilized a time interval of [0, 15] seconds and considered the initial values for v_0 and β_0 from the data presented from 4.32 to 4.40.

The ode45 function, designated "Solve nonstiff differential equations with a medium order method," is available in MatLab and can be applied to a variety of differential equations [41]. The format of the ode45 function can be customized to the specific variables required for the equation in question. Examples of the ode45 formats can be found in the reference at 4.2.

```
[t,y] = ode45(odefun,tspan,y0);
[t,y] = ode45(odefun,tspan,y0,options);
[t,y,te,ye,ie] = ode45(odefun,tspan,y0,options);
```

Ode45 formats 4.2: MATLAB ode45 examples. (Source: [41])

In the case of the developed code, we used β_0 and v_0 as inputs for ode45. Once the values have been resolved, the corresponding variables must be extracted. This is achieved by retrieving the values from β and w. Extracting these values depends on the naming used in the ODE, as explained in reference 4.1. The structure used should be similar to that shown in reference 4.44 and 4.45.

$$w = y(:, column) \tag{4.44}$$

$$\beta_0 = y(:, column) \tag{4.45}$$

We will obtain the set of solutions, y, by solving ode and ode45 and considering the output of the solutions, which will consist of two columns. We will extract the values based on whether they are in the first or second column. Ensuring that the order used to extract the results is equivalent to the order defined and used in ODE is important.

Once the values have been extracted, we will plot the results, in particular the graphs that will be presented below in the sub subsection **Results and Discussion** 4.2.1.2, as well as the dynamic graph where we can see the evolution of the trajectory over time, thus giving us a direct view of what is happening in the code.

A plot was made of the angular velocity, which in this case represents the velocity w over time t in seconds, and a graph of the angle β over time t. The purpose of using these graphs is to check whether the evolution of the velocity w and the angle β is in line with what was expected and whether what we observe graphically is in line with what we observe through the dynamic graph. The plot of these graphs follows a simple structure similar to that presented in 4.3.

```
figure;
```

```
subplot(2,1,1);
plot(tempo, velocidade_angular, 'b-', 'LineWidth', 1.5);
title('Velocidade Angular ao Longo do Tempo');
xlabel('Tempo (s)');
ylabel('Velocidade Angular (deg/s)');
grid on;

subplot(2,1,2);
plot(tempo, angulo, 'r-', 'LineWidth', 1.5);
title('Angulo ao Longo do Tempo');
xlabel('Tempo (s)');
ylabel('Angulo (rad)');
grid on;
```

Code Structure 4.3: Code of the plot for the graphics.

The trajectory of the kite over time is represented by a dynamic graph with a more complex structure compared to ordinary plots. In order to create a dynamic graph, it was necessary to define the size of N, which will be used for the for loop that will update the position of the pendulum over time. The value of N will determine the size of the time steps, which in this case is the size of the vector containing the β values. Once the size of N has been defined, a new figure is created and the origin, which serves as the pivot of the pendulum, is defined and plotted. Subsequently, the iterative cycle is created, which will update the positions in x and z over time, considering the values obtained through the calculations and updating them at the end of each iteration. This approach allows for observing the entire trajectory of the pendulum from the commencement of the simulation to its conclusion. The fundamental structure employed to generate the dynamic graph is analogous to that depicted in 4.4.

```
N = length(beta);

figure(2);
clf
plot(0, 0, 'ro', 'MarkerSize', 10, 'MarkerFaceColor', 'r');

for i = 1:N

x = L * cos(beta(i));
z = -L * sin(-beta(i));

hold on;
plot(x, z, 'k>', 'MarkerSize', 10, 'MarkerFaceColor', 'k');

pause(dt);

drawnow;
\end
```

Code Structure 4.4: MATLAB code for pendulum simulation

It is crucial to consider the impact of wind, represented as v_w, on the code, and modify the equations accordingly. Instead of relying on the original F_D equation, which assumes that wind does not impact the calculations, it is now necessary to incorporate the difference described in equation 4.29. This modification will lead to the equation previously introduced in equation 4.30.

The code has been updated to include the wind speed value, v_w, set at $5m/s$, as part of the parameters. This modification also alters the previously used F_D. Initially, the system of equations referenced in 4.22 was solved using the ode45 solver with a wind speed of $5m/s$.

However, the results exhibited unusual behavior, suggesting potential issues with the use of ode45. In response, adjustments were made to solve the optimization problems using other ODE solver variants, such as ode23s and ode15s, which are more robust and capable of handling both stiff and non-stiff problems.

Stiff problems occur when a system of differential equations has components that change rapidly alongside those that evolve slowly. This leads to some parts of the system having very large derivatives (slopes), while others progress at a much more gradual rate. In such scenarios, explicit ODE solvers like ode45 may require prohibitively small time steps to maintain stability, even when the overall behavior of the system does not demand such precision. This inefficiency can be addressed by employing solvers specifically designed to manage stiffness, such as ode15s, ode23s, or ode23t. A practical way to illustrate this concept is through an electrical circuit that features significant differences in time constants. For example, we can observe components that respond quickly, like capacitors, alongside those that respond slowly, such as inductors.

In contrast, non-stiff problems can be effectively solved using explicit methods like ode45, which can accommodate reasonable step sizes. These systems do not display extreme variations in their components, allowing the solver to handle them efficiently without the necessity for excessively small time steps. A prime example of this concept is simple harmonic oscillators, which are systems where the solution changes smoothly and does not involve significant differences in time scales.

Nevertheless, the results were still not as expected. As a final attempt to apply ODE directly, the code was divided into smaller parts, and "options" were used with tolerance adjustments. However, as the use of ODE limits the understanding of what is actually happening, these adjustments proved to be inadequate to solve the problem. In order to incorporate the code relating to the introduction of wind, we developed a new code from scratch. This time, we manually and interactively integrated everything. This approach provided us with a deeper understanding of the process, making debugging easier.

To begin implementing the new code, as mentioned earlier, the first step is to initially declare all the parameters. An additional parameter for wind, represented by v_w with a magnitude of 5 m/s, has been introduced. The declaration of the parameters and their corresponding values can be found in equation 4.46 to 4.55. It is important to highlight that we will be conducting

different tests using wind. The first test will involve a wind speed of 5 m/s working in favor, while the second test will involve a wind speed of -5 m/s working against. These tests will help us understand the impact of wind direction on the motion of the kite and the resulting angular velocity and angle graphics. These minor adjustments will only affect specific parameters, while the rest of the code will remain unchanged.

$$\rho = 1.223\,\text{kg/m}^3 \tag{4.46}$$
$$A = 0.7\,\text{m}^2 \tag{4.47}$$
$$m = 0.4\,\text{kg} \tag{4.48}$$
$$C_D = 0.05 \tag{4.49}$$
$$C_L = [1.7, 2.4] \tag{4.50}$$
$$L = 1.3\,\text{m} \tag{4.51}$$
$$g = 9.81\,\text{m/s}^2 \tag{4.52}$$
$$\beta_0 = -\frac{\pi}{2} \tag{4.53}$$
$$v_0 = 0.001\,\text{m/s} \tag{4.54}$$
$$v_w = \pm 5\,\text{m/s} \tag{4.55}$$

We began by establishing the number of steps, denoted as n_{steps}, at 100 steps per second. The time per step, represented as d_t and calculated like $\frac{1}{n_{steps}}$. The final simulation time was defined as $t_{final} = 15$ seconds. It is also important to define the total simulation time, t_{total}, so that we can set up the loop for iterations and manual updates. The structure employed is analogous to that presented in 4.56 to 4.59.

$$n_{steps} = 100 \tag{4.56}$$
$$d_t = \frac{1}{n_{steps}} \tag{4.57}$$
$$t_{final} = 15 \tag{4.58}$$
$$t_{total} = 0 : d_t : t_{final} \tag{4.59}$$

In the next step, we need to define and initialize a vector, which we will call y. This vector will contain the angle and angular velocity values. Since we are only interested in the angle β and the angular velocity w, the vector will have two columns. We will start by entering zeroes in both columns and then in the first row, we will initialize the values based on the parameters [β_0, v_0], as shown in 4.60 and 4.61.

$$y = zeros(lenght(t_{total}, 2)) \tag{4.60}$$

$$y(1,:) = [\beta_0, v_0] \tag{4.61}$$

After defining parameters and initializing, we will set up a loop for iterations. The loop will continue as long as t is less than the size of t_{total} - 1. We remove the first position because the iterations start from it, so we avoid repeating values. The appearance of the vector y, given a defined size of $t_{total} - 1$, will be similar to what we can see in figure 4.5.

	Vetor y	
	Angle	Angular Velocity
t = 1	β_0	v_0
t = 2		
t = 3		
t = 4		
	⋮	⋮
t = lenght(t_{total})-1		

Figure 4.5: Vector y.

Within the loop, we will retrieve the current values of β and velocity, and then calculate the drag force, F_D, using the formula presented in 4.30. We also determine the force F_P, which depends on the angular velocity w as mentioned in 4.24.

After defining the forces, we will calculate the acceleration using the formula 4.22. Then, we integrate this acceleration to obtain the next speed and angle. This process enables us to update the current velocity and angle values by adding the newly calculated values to the previous ones and saving them in the next position of the vector, at position t+1.

This process of removing, calculating, updating, and saving values will continue until the total loop time is reached. The structure explaining how the loop works can be found in the algorithm 1.

Finally, to verify the results, we created graphs of angular velocity, angle, and dynamics. The structure and code are almost identical to the previously presented code in 4.3 and 4.4.

Algorithm 1 : Kite Pendulum Simulation in 2D

for $t \leftarrow 1$ to $length(t_{total}) - 1$ **do**
  $\beta \leftarrow y(t,1)$ ▷ Current angle
  $w \leftarrow y(t,2)$ ▷ Current angular velocity
  $F_P \leftarrow 1$ ▷ Push Force Magnitude
  $F_D \leftarrow 0.5 \times \rho \times A \times C_D \times (w - vw)^2$ ▷ Drag Force
  $F_P \leftarrow (w > 0) \times F_P$ ▷ Push Force
  $a \leftarrow \frac{F_P - F_D - m \times g \times \cos(\beta)}{m}$ ▷ Acceleration
  $w_{\text{next}} \leftarrow w + dt \times a$ ▷ Update angular velocity
  $\beta_{\text{next}} \leftarrow \beta + dt \times w$ ▷ Update angle
  Store results: $y(t+1,1) \leftarrow \beta_{\text{next}}$
  Store results: $y(t+1,2) \leftarrow w_{\text{next}}$
end for

4.2.1.2 Results and Discussion

This section contains the results obtained from the previously described implementation and provides a discussion of these results.

The analysis initially focuses on the movement of the kite without considering the influence of the wind. The first graph illustrates the dynamic movement of the kite over time, represented by a triangle pointing in the positive direction of the trajectory. Starting at position -$\frac{\pi}{2}$ rad with an initial positive velocity of v_0 = 0.001 m/s, the kite experiences a push force, F_P, of magnitude 1, activating the motor and causing it to move slightly in the positive direction. Subsequently, it reverses in a rocking motion to the negative direction, no longer influenced by F_P. This oscillating motion occurs repeatedly, resembling a pendulum being pushed, and results in a continual increase in speed. The movement graph eventually indicates that the kite has reached a sufficient speed and is following a systematic circular trajectory. This behavior aligns with expectations: the kite initially performs a pendulum movement and then progressively increases its speed to move along a circular path. The kite is ready to enter the energy production phase and the flight envelope at this stage.

In figure 4.6, we can see the motion graph illustrating the various trajectories taken by the kite within the defined time period of 15 seconds.

After analyzing the movement graph, we will conduct a more thorough examination of the variations in angle and speed to ensure that the graphs accurately depict our observations.

The graph in figure 4.7 displays the angular velocity w of the kite without the influence of wind. Initially, we observe a slight positive variation due to the push force, F_P, and the initial positive velocity followed by a change in direction as seen in the dynamic graph 4.6. The kite transitions between positive and negative speeds due to its rocking movement, consistently increasing its speed and variation. Around t = 5.98 seconds, the kite experiences an exponential increase in speed, which can be attributed to reaching the necessary speed to begin describing a circular trajectory. After 4.02 seconds, the kite stabilizes its movement. From t = 10 seconds, the speed variation remains nearly constant, reaching peaks of 400 rad/s with waves having an amplitude of

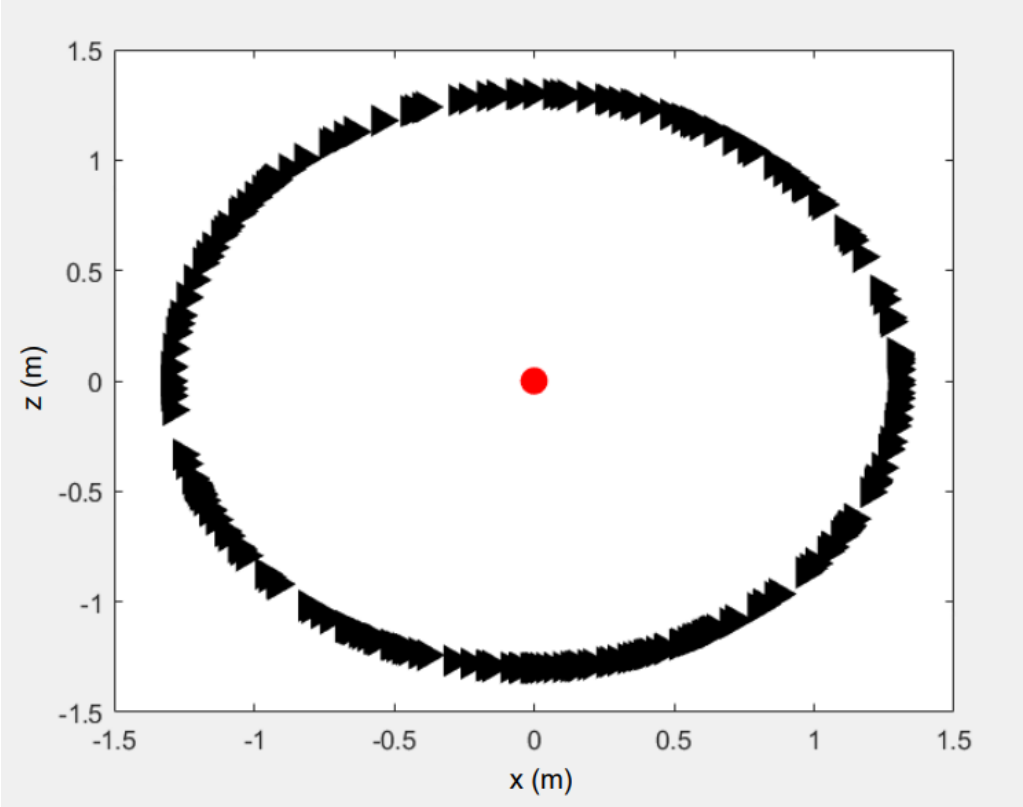


Figure 4.6: Graph showing the kite dynamic over time.

approximately 100 rad/s and a period of about 1.44 seconds. These results align with expectations from observing the movement graph.

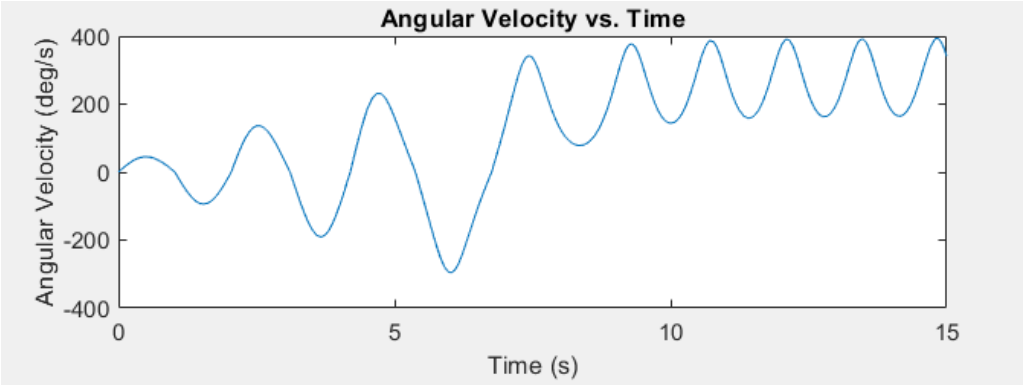


Figure 4.7: Graph showing the angular velocity of the kite over time.

After analyzing the graph showing the angular velocity, we created a graph that illustrates the variation of the angle β in degrees. This graph is represented in figure 4.8, and it shows how the angle β changes over a 15-second interval. As explained in section 2.7.2.1, the angle β is the angle between the position of the kite and the x-axis. Initially, the angle variation between positive and negative is an almost imperceptible change, likely due to the low speed of the kite.

As the speed increases, the angle also increases proportionally, as indicated by the relationship between angular velocity and angle. This relationship is more noticeable when both graphs are considered together. It is apparent that from the moment the speed undergoes a rapid increase at t = 5.98 seconds, the angle also rises rapidly. This trend continues even after the kite reaches a constant speed.

The rapid increase in the angle even after the kite reaches a steady state in the angular velocity graph (see Figure 4.7) can be explained by the fact that the kite is completing successive full turns. If we consider that with each full turn the kite describes a cycle from 0º to 360º (0 to $2 \times \pi$ rad) and that it has completed n full turns, the angle variation and its maximum value will always increase with each cycle. We can then define the maximum value that the angle β reaches within an interval of 0º to 360º $\times n$ (0 to $2 \times \pi \times n$ rad). This interval represents the maximum value of the angle, which depends on the number of complete turns the kite has made n. We estimate that the kite has completed 5 full turns. Therefore, the maximum value observed in the 15-second interval is 1800 degrees, which is approximately what we see in the graph (360º $\times$ 5 = 1800º).

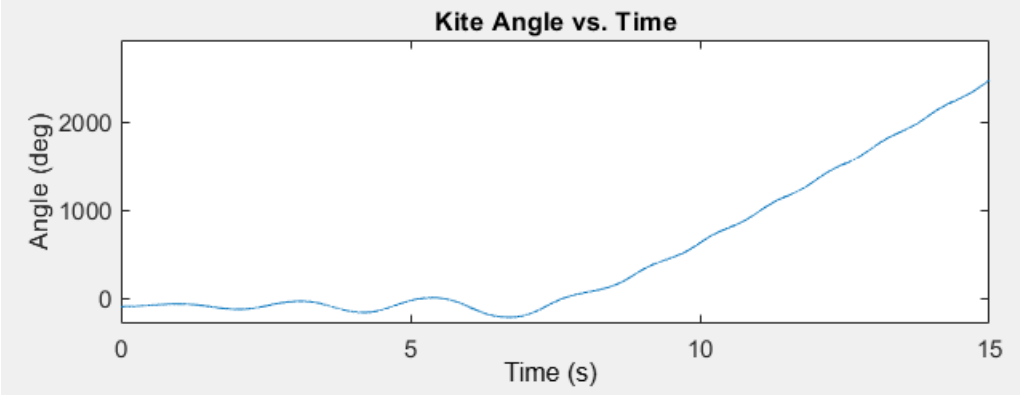


Figure 4.8: Graph displaying the results of changing the angle β in degrees.

Now that an initial analysis has been completed without considering the influence of the wind, we will carry out an analysis considering the wind in two different situations. First, we will analyze the impact of the wind blowing in the direction of the x-axis, and then we will consider the wind blowing in the opposite direction (the negative direction of the x-axis).

The first situation we will analyze is when the wind is in our favor. As mentioned earlier in the implementation, we considered a wind speed of 5 m/s ($v_w = 5m/s$), and we will analyze its impact on the angular velocity and angle graphs, as well as the dynamic graph.

The first graph we are analyzing is the kite dynamics graph. This dynamic graph gives us an idea of the trajectory that the kite takes over a 15-second period. By observing the graph labelled 4.9, we can see that when the wind is favorable, the kite moves in a pendulum motion and gradually increases its speed until it reaches enough speed to describe a circular trajectory. The strong wind and the initial push force (because of the initial positive velocity) propel the kite forward with minimal resistance from drag force, enabling the kite to almost immediately begin

moving in a circular trajectory. In this situation, the pendulum motion is not observed. The vertex on the edge of the triangle indicates the positive direction of the trajectory, as mentioned before.

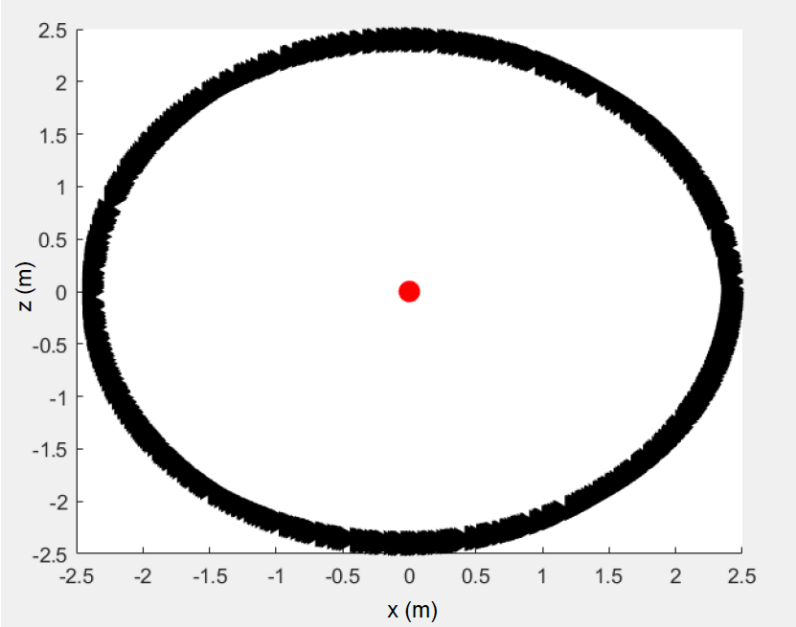


Figure 4.9: Graph showing the kite dynamic over time in response to the wind in favor.

The next graph to be analyzed is the angular velocity graph, where we can observe the performance of velocity and determine if its behavior matches what we observed in the dynamic graph. Looking at figure 4.10, we can see that the speed increases rapidly and then continuously oscillates in a positive direction. One reason for this sudden increase could be the presence of a positive initial velocity, v_0. The repeated peaks in oscillations can be attributed to the kite quickly initiating a circular trajectory and gradually increasing its velocity with each full turn until it reaches a stable state, at which point it maintains a constant velocity. The kite promptly adopts a circular trajectory due to the strong wind, the influence of the push force, F_P, and the minimal resistance caused by the drag force, F_D. From approximately t = 8 seconds, the velocity enters a steady state, oscillating with a constant amplitude. This behavior may be attributed to the kite beginning to make consistent full turns at a steady speed, signaling its readiness to enter the energy production phase. The graph shows promising results, indicating that wind has a positive impact on the angular velocity of the kite. It also highlights that when the wind speed is favorable, the kite accelerates more quickly, reaching equilibrium faster compared to when unaffected by the wind.

In the final graph of the upwind speed test, we will examine the angle β. The graph 4.11 shows a significant increase in the angle almost immediately. Similar to the velocity, the kite does not undergo the swinging movement and instead begins a circular trajectory. As a result, the angle continues to increase with each complete turn. Upon observing the graph at 15-minute intervals, it is evident that the maximum angle β reaches approximately 9000 degrees, which is equivalent to about 25 full turns. The range of the angle follows the pattern of 0º to 360º $\times n$ (or 0 to $2 \times \pi \times n$ radians), where n is the number of turns, as mentioned earlier. This increase indicates that the

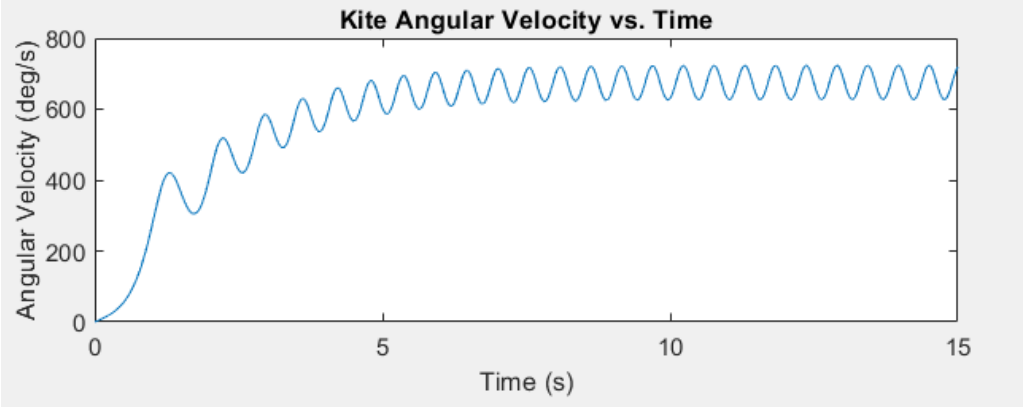


Figure 4.10: Graph showing the angular velocity of the kite over time in response to the wind in favor in deg/s.

kite consistently gains angular velocity with each complete turn. When the wind is favorable, the angle reached is significantly higher compared to when there is no strong wind. Without the wind, the angle reaches approximately 1800, whereas, with the wind in its favor, the angle reaches 9000 degrees—marking a fivefold increase $\frac{9000}{1800} = 5$. The wind greatly assists the kite in increasing its velocity and rapidly reaching the necessary speed to initiate the production phase.

In an ideal scenario, we only consider forces in the angular direction with a constant wind speed and direction. However, in real-world conditions, the graphics would be different due to varying wind directions and speeds, which can impact the kite and the graphics. Additionally, the forces that are in equilibrium in the radial direction can also significantly influence the graphics when there is no equilibrium in the radial direction, making this force important and impactful on the graphics as well.

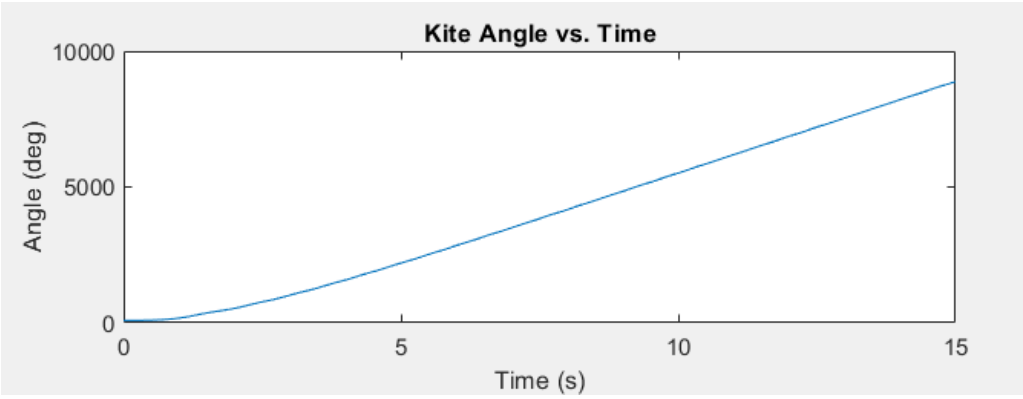


Figure 4.11: Graph showing the impact of the favor wind on the change in angle β in degrees.

Now, we will test the impact of the against wind on the kite and examine the graphs again. We will assume the wind speed to be -5 m/s.

The kite begins at the position of $-\frac{\pi}{2}$ radians and initially gains positive speed due to the initial speed, v_0, and the activating of the push force, F_P. However, it then changes its trajectory and repeats this motion without completing a full turn, unlike the previous scenario. In this case,

the kite is caught in a constant pendulum motion. The influence of the headwind, instead of aiding the speed of the kite like a tailwind would, acts as a resisting force, causing the kite to engage in a constant swinging motion whenever it tries to gain speed. The headwind and the drag force work as resistance forces, hindering the speed increase of the kite.

We can analyze the graph in figure 4.12 to observe the variations in angular velocity. Initially, the kite displays a small angular velocity in the positive direction, but it later oscillates due to the sustained influence of the headwind. This behavior parallels that of a pendulum system, with the kite functioning as the pendulum. Furthermore, the opposing wind introduces a drag force that directly impacts the motion of the kite. The peaks in angular velocity correspond to the kite reaching its maximum displacement in any direction, with the angular velocity going to zero when the kite changes direction. The consistent amplitude suggests that the system is in a quasi-stationary state, where the forces are balanced, allowing continuous oscillations. The resistance force from the opposite direction of the wind is not strong enough to completely stop the oscillations and make the system complete a full turn due to the push force that is activated in the positive velocity direction. If the wind is against the kite and the speed is insufficient to complete the turn, the kite becomes stuck in a pendulum motion.

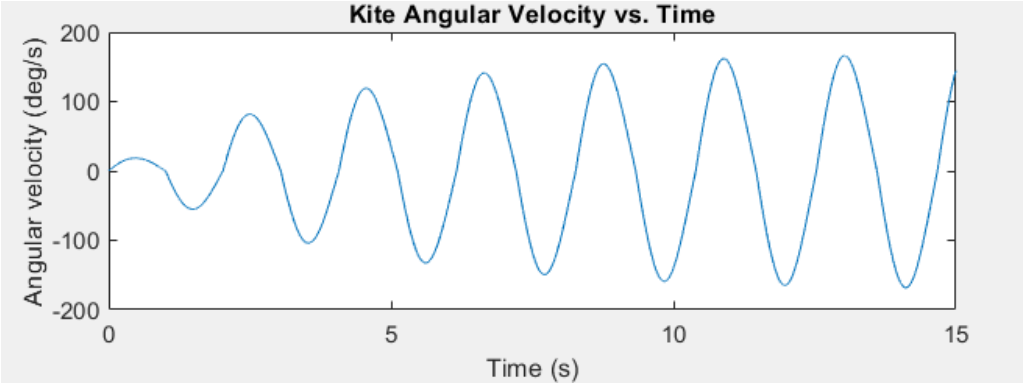


Figure 4.12: Graph showing the angular velocity of the kite over time in response to the opposing wind in deg/s.

The graph in Figure 4.13 illustrates that the kite undergoes continuous oscillatory motion, swinging back and forth without significantly increasing the angle.

Observing the graph of the angle β, we notice a pattern similar to that of the angular velocity graph. The kite appears to be in a pendulum-like motion due to opposing forces that effectively cancel each other out. This creates a situation in which the wind acts as an additional resistive force alongside the drag force (F_D), preventing the kite from completing a full rotation and entering the energy production phase. This happens even though the push force (F_P) operates in the positive direction of the velocity, aimed at propelling the movement forward. Starting from an initial position of -$\frac{\pi}{2}$ radians (-90 degrees), the kite varies its angle but never completes a full rotation. This behavior can be directly compared to the angular velocity graph, where the kite oscillates between positive and negative speeds without gaining the momentum needed to complete a full

turn. Consequently, the kite remains on a trajectory reminiscent of the movement patterns observed in the simple pendulum tests discussed earlier in section 3.

One effective method for liberating the kite from its constant pendulum motion is to adjust the values of the arbitrary push force F_P. By increasing this force, the kite can gain the necessary speed to initiate a circular path and enter the production phase, even when faced with additional resistance from opposing winds. Additionally, increasing the initial velocity v_0, in conjunction with the push force F_P, can further facilitate the transition of the movement of the kitr from a pendulum swing to a circular trajectory.

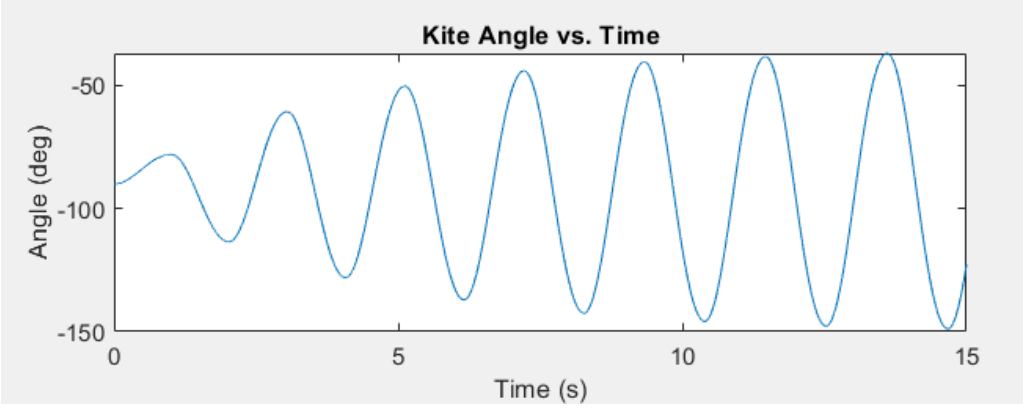


Figure 4.13: Graph showing the impact of the opposing wind on the change in angle β in degrees.

Upon reviewing the results, it is evident that wind significantly affects the outcome. A comparison between the influence of upwind and no wind shows that the kite can achieve higher speed and initiate a circular trajectory more rapidly when supported by the wind. When comparing the graphs for upwind and against, it becomes apparent that the kite struggles to reach sufficient speed and initiate a circular trajectory when faced against the wind, resulting in an oscillatory movement. Based on the results, it is favorable to have the wind supporting the kite to achieve higher speeds, enabling the kite to descend along the circular path more efficiently and progress to the flight stage. Furthermore, the direction in which the wind hits the kite, whether from the back or the wings, can either facilitate take-off or act as a force slowing it down. These variables in the real environment can influence outcomes by inducing changes in the parameters.

Incorporating realistic conditions into simulations could enhance the credibility of the results. However, doing so would add complexity to control and predictions, as current simulations rely on oversimplifications that overlook real-world factors.

In a real-time scenario, the dynamics would differ slightly. It would be essential to account for the forces acting in the radial direction, along with various environmental and physical variables, including the continual changes in velocity direction and variable speeds, which could significantly affect the overall graphical representation.

4.2.2 3D Dimensions

The focus of our previous simulations was on 2D scenarios. Now, we are shifting our attention to 3D simulations. In these simulations, the wind direction will be positioned along the y-axis, perpendicular to the xz plane. This change completely alters the previous formulas and code implementation used in the 2D work.

Formulating the equations for 3D simulations requires a redefinition of certain angles and the consideration of multiple perspectives and projections on the planes. This complexity arises from introducing a completely new viewpoint, prompting an examination of the directions of the various forces. While these forces have slight differences, they bear strong similarities to those already defined in the 2D simulations.

As discussed in subsection 2.7.2.2, we explore the coordinate frame used and gain an overview of the various perspectives considered.

The initial perspective in developing the mathematical formulas involves the projection of the kite onto the yz plane, which is illustrated in figure 4.14. In the diagram, as mentioned earlier, we can observe the side view when the wind blows perpendicular to the kite, causing it to tilt. The angle of tilt remains constant because the wind is consistently blowing at the same angle.

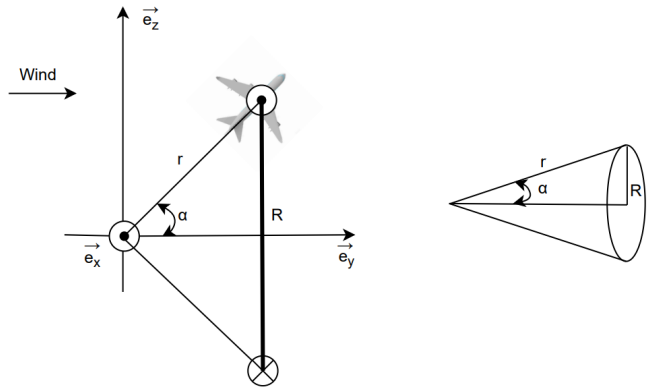


Figure 4.14: Visual representation of the kite in the yz plane. (Source: [16])

By analyzing the previous diagram, we can derive the relationships that are directly linked to the radius of the circle formed by the kite in the frontal view. These equations will be used for calculations from the frontal view perspective and can be derived using the relationship described in Equation 4.62.

$$R = r \cdot \sin(\alpha), \alpha = constant \tag{4.62}$$

In this scenario, we are considering a constant value, denoted as α, which we will set to an arbitrary value of $\frac{\pi}{3}$ radians. We are also looking at the size of a rope, denoted as r. By using the sine function, we can determine the radius of the circle, R.

Once we establish this relationship, we project the forces onto the xz plane to obtain a front view of the circular motion. The motion starts with the kite making the pendulum movement, which, after reaching sufficient speed, starts making a complete circumference. This allows us to easily project the forces and obtain the mathematical relationships that form the basis for implementing the controller.

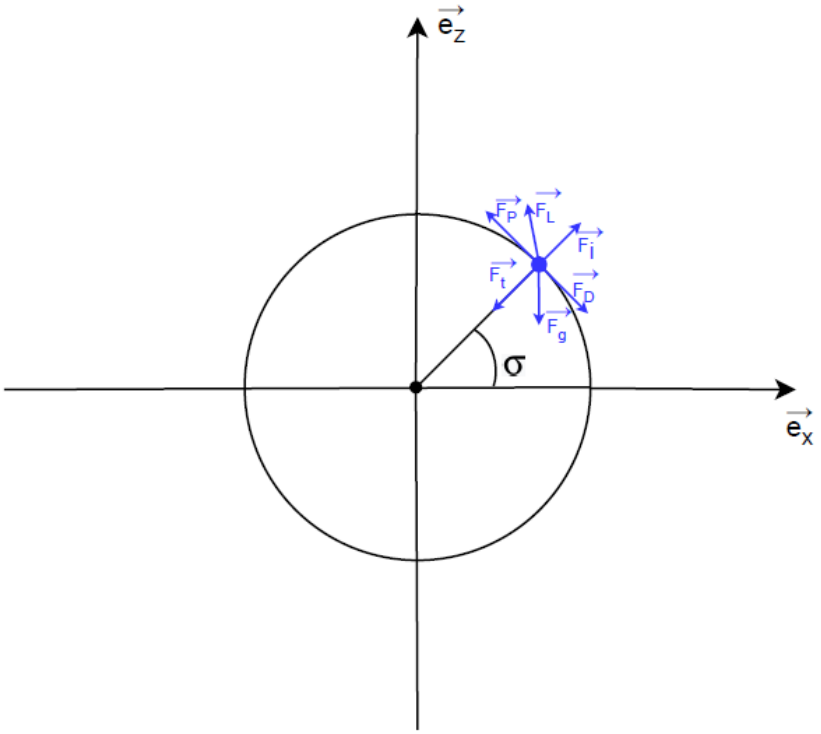


Figure 4.15: Visual representation of the forces on the plane xz.

In Figure 4.15, we observe the projection of forces on the xz plane. From these projections, we can establish the mathematical relationships governing the forces. The angle σ, measured between the position of the kite and the x-axis, varies as the kite moves along its trajectory on the xz plane. We can also discern the direction of the forces, most of which align with previously presented forces. These include the tangential force, F_t, along the rope, the gravitational force, F_g, representing the weight of the kite, the inertial forces, F_i, that counteract the tangential force, and the push, F_P, and drag forces,F_D, that oppose each other along the trajectory. The push force acts in the positive direction of the trajectory, while the drag force acts in the negative direction. Lastly, the lift force (F_L), pointing upwards, facilitates the elevation and varies with the body coordinates of the kite. The velocity vector $\vec{v}$ aligns with the trajectory and is defined in Equation 4.63.

$$\vec{v} = -v \cdot \sin(\sigma) \cdot \vec{e_x} + v \cdot cos(\sigma) \cdot \vec{e_z} \tag{4.63}$$

In equations 4.64, 4.65, 4.66, and 4.67, we observe the kite equations derived from force decomposition and projection onto the xz plane.

$$\overrightarrow{F_g} = -F_g \cdot \overrightarrow{e_z} \tag{4.64}$$

$$\overrightarrow{F_P} = -F_P \cdot sin(\sigma) \cdot \overrightarrow{e_x} + F_P \cdot cos(\sigma) \cdot \overrightarrow{e_z} \tag{4.65}$$

$$\overrightarrow{F_D} = F_D \cdot sin(\sigma) \cdot \overrightarrow{e_x} - F_D \cdot cos(\sigma) \cdot \overrightarrow{e_z} \tag{4.66}$$

$$\overrightarrow{F_i} = F_i \cdot cos(\sigma) \cdot \overrightarrow{e_x} + F_i \cdot sin(\sigma) \cdot \overrightarrow{e_z} \tag{4.67}$$

These are the main equations that we can derive from the projection of the kite on the xz plane. It is also possible to calculate the tangential force, but it requires the use of local coordinates since the tangential force aligns with the direction of the rope but opposes the direction defined by e_r, which represents the radial direction. The tangential forces are defined using local coordinates because they are components in the global coordinate system in the three axes. In figure 4.15, we can see the orientation of the vector $\overrightarrow{e_r}$ and the force F_t by projecting the forces onto the yz plane.

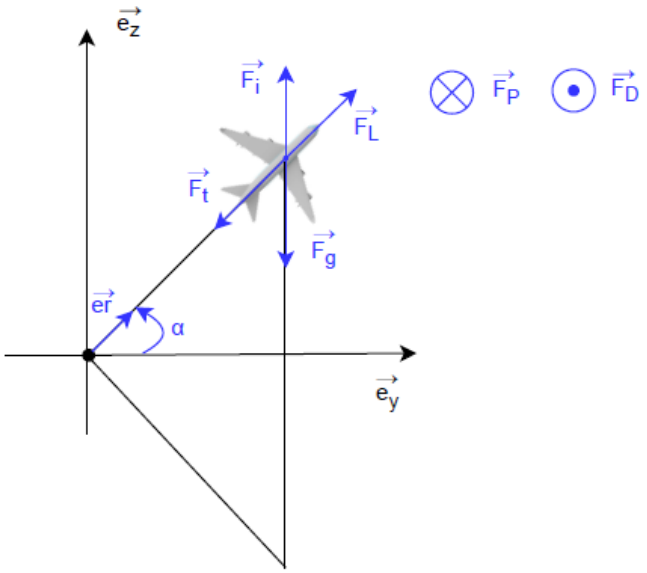


Figure 4.16: Visual representation of the forces acting on the kite in the plane yz. (Source: [16])

In this way, we can determine the force F_t using the equation in 4.68.

$$\overrightarrow{F_t} = -F_t \cdot \overrightarrow{e_r} \tag{4.68}$$

It is important to convert the local coordinates into global coordinates in order to find the tangential force F_t in the x, y, and z components, as we are working with global coordinates instead of local coordinates. This conversion can be achieved using the transformation matrix presented in 4.69.

$$\begin{bmatrix} e_x \\ e_y \\ e_z \end{bmatrix} = \begin{bmatrix} \sin\left(\frac{\pi}{2}-\beta\right)\cdot\cos(\phi) & \cos\left(\frac{\pi}{2}-\beta\right)\cdot\cos(\phi) & -\sin(\phi) \\ \sin\left(\frac{\pi}{2}-\beta\right)\cdot\sin(\phi) & \cos\left(\frac{\pi}{2}-\beta\right)\cdot\sin(\phi) & \cos(\phi) \\ \cos\left(\frac{\pi}{2}-\beta\right) & -\sin\left(\frac{\pi}{2}-\beta\right) & 0 \end{bmatrix} \begin{bmatrix} e_r \\ e_\beta \\ e_\phi \end{bmatrix} \tag{4.69}$$

When we apply this transformation matrix, since we only have one component e_r, which is the magnitude of F_t in the negative direction, we will have the transformation shown in 4.70, and then after the simplifications, the result presented in 4.71.

$$\begin{bmatrix} e_x \\ e_y \\ e_z \end{bmatrix} = \begin{bmatrix} \cos(\beta)\cdot\cos(\phi) & \sin(\beta)\cdot\cos(\phi) & -\sin(\phi) \\ \cos(\beta)\cdot\sin(\phi) & \sin(\beta)\cdot\sin(\phi) & \cos(\phi) \\ \sin(\beta) & -\cos(\beta) & 0 \end{bmatrix} \begin{bmatrix} -F_t \\ 0 \\ 0 \end{bmatrix} \tag{4.70}$$

$$\begin{bmatrix} e_x \\ e_y \\ e_z \end{bmatrix} = \begin{bmatrix} -F_t\cdot\cos(\beta)\cdot\cos(\phi) \\ -F_t\cdot\cos(\beta)\cdot\sin(\phi) \\ -F_t\cdot\sin(\beta) \end{bmatrix} \tag{4.71}$$

In this manner, we are able to obtain the force across the three components x, y, and z, as illustrated in 4.72.

$$\overrightarrow{F_t} = -F_t\cdot\cos(\beta)\cdot\cos(\phi)\cdot\overrightarrow{e_x} - F_t\cdot\cos(\beta)\cdot\sin(\phi)\cdot\overrightarrow{e_y} - F_t\cdot\cos(\beta)\cdot\overrightarrow{e_z} \tag{4.72}$$

After analyzing the obtained result, we noticed that the x, y, and z components of these equations depend on the angles β and ϕ. However, in the projections made on the planes, these angles are not directly available. The angle that we can obtain from the projections and calculations is the σ angle. Therefore, we need to determine the angles β and ϕ in terms of the angle σ. This logic is similar to the one illustrated in figure 4.17.

In this way, we can express the mathematical relationship between the angles β, ϕ, and the angle σ. Equations 4.73 and 4.74 demonstrate the mathematical relationships found in the article [42].

$$\beta(\sigma) = \beta_0 + \Delta\beta\cdot\sin(\sigma) \tag{4.73}$$

$$\phi(\sigma) = \Delta\phi\cdot\cos(\sigma) \tag{4.74}$$

In the following formulas, we have the angle β_0, which is chosen arbitrarily, and $\Delta\beta$, which is also given. For simplicity, we assume that $\Delta\beta$ is equal to $\Delta\phi$. This allows us to replace the angles involved in calculating the force F_t and determine its value based on the angle σ, which should fall within the range of $[0, 2\times\pi]$.

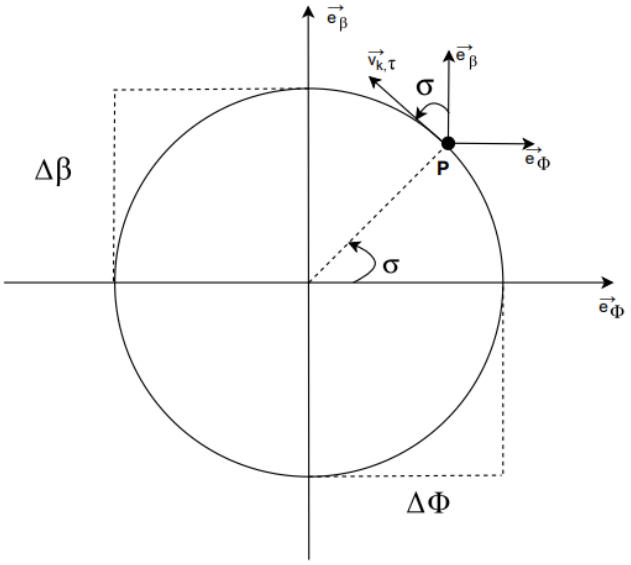


Figure 4.17: Kite circular trajectory within the tangent plane.

The final force we need to calculate is the lift force F_L. This force depends on the body coordinates of the kite. The force F_L will be in the opposite direction to the force e_{yaw}, which controls the vertical movement and has a negative direction. Because the lift force works to help the kite rise, the coordination of the body is important for controlling its vertical movement and increasing its altitude. The figure 4.18 illustrates the system of body coordinates previously explained in 2.7.2.2.

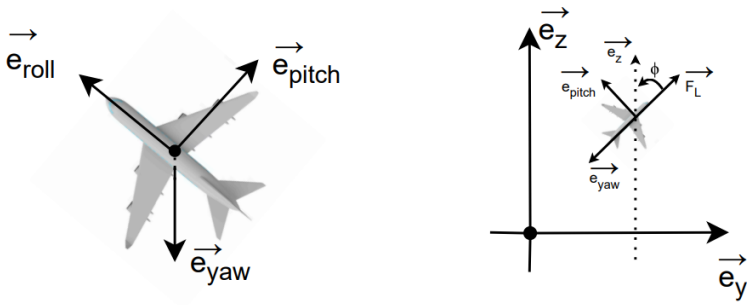


Figure 4.18: Body coordinates System (Source: [16])

As the lift force opposes e_{yaw} by aiming to elevate the kite, we can derive the lift force equation shown in 4.75.

$$\vec{F_L} = -F_L \cdot \vec{e_{yaw}} \tag{4.75}$$

Even though we have already obtained the equation for the lift force (F_L), we still need to compute e_{yaw}, which constantly changes and is influenced by the other body coordinates e_{roll} and e_{pitch}.

We will start by calculating the coordinate e_{roll}. Since e_{roll} governs the longitudinal movement, we can establish a relationship and determine it by normalizing the velocity vector, as shown in equation 4.76, under the assumption that they are aligned.

$$e_{roll} = \frac{\overrightarrow{v}}{\|\mathbf{v}\|} \tag{4.76}$$

In the figure 4.18, we can observe that the roll angle is measured between the lift force and the z-axis, and it serves as an activation variable. When the roll angle is 0, we have e_{yaw} = -e_r and e_{pitch} varies between e_β and e_ϕ. If the roll angle is not 0, we can assume that it falls between e_{pitch} and e_β, e_ϕ.

By combining the local coordinates and the roll angle, we can determine e_{pitch} and e_{yaw}.

The calculation of e_{pitch} involves using the Rodrigues formula to obtain the rotation matrix as presented in 4.77.

$$e_{pitch} = \mathbf{v} \cdot \cos\theta + (\mathbf{k} \times \mathbf{v}) \cdot \sin\theta + \mathbf{k} \cdot (\mathbf{k} \cdot \mathbf{v}) \cdot (1 - \cos\theta) \cdot \|\mathbf{v}\| \tag{4.77}$$

We have $\mathbf{v}$ as the original vector, $\mathbf{k}$ as the unit vector along the axis of rotation, and θ as the angle of rotation. The symbol $\times$ denotes the cross product, and $\cdot$ denotes the product. By applying this rotation matrix and modifying it for the variable in the context of our problem, we can obtain our e_{pitch}.

After obtaining our e_{pitch}, and since we already have the e_{roll}, we can obtain the e_{yaw} through the cross product, as shown in equation 4.78.

$$e_{yaw} = e_{roll} \times e_{pitch} \tag{4.78}$$

The lift force (F_L) will now depend on the result for the e_{yaw} coordinate.

Now that we have the forces F_P, F_D, and F_L, we can determine the velocity, which is important for graphing and verifying results. We can calculate the velocity by applying the second law of Newton, which states that the sum of all the forces is equal to $m \cdot \dot{\mathbf{v}}$. The equation shown in 4.79 will illustrate the relationship that allows us to calculate the acceleration and, subsequently, the velocity, v. It is important to note that, similar to 2D perspective calculations, we are assuming that other forces acting on the kite, such as tangential force, inertial force, and gravitational force, are in equilibrium and do not significantly affect speed calculation. We only take into account the forces directly influencing the trajectory and velocity, such as push, drag, and lift forces that help elevate the kite. It is important to emphasize that in real-time conditions, we must consider all forces that impact the calculations, especially those not in equilibrium, and environmental conditions such as wind direction and intensity, which also play a crucial role.

$$m \cdot \dot{\mathbf{v}} = F_P + F_L - F_D \tag{4.79}$$

Note that by integrating the speed v, we can calculate the position of the kite x along the trajectory. This information can be helpful for further investigation to observe the trajectory of the kite.

Like in the 2D perspective, the magnitude of the push force in the 3D perspective was chosen arbitrarily (4.81), while the other magnitudes depend on the formulas presented in 4.80, 4.82, 4.83, and 4.84.

$$F_g = m \cdot g \tag{4.80}$$

$$F_P = \begin{cases} 1 & \text{if } v > 0 \\ 0 & \text{if } v \leq 0 \end{cases} \tag{4.81}$$

$$F_D = \frac{1}{2} \cdot \rho \cdot A \cdot C_D \cdot v^2 \tag{4.82}$$

$$F_L = \frac{1}{2} \cdot \rho \cdot A \cdot C_L \cdot v^2 \tag{4.83}$$

$$F_i = \frac{m \cdot v^2}{R} \tag{4.84}$$

The calculation of magnitudes is essentially the same as in 2D calculations. The main difference is in calculating the inertial forces, which now depend on the radius R of the circle instead of the length of the rope. Additionally, for more realistic results, if we want to consider all the forces acting on the kite, we need to calculate the magnitude of the tangential force (F_t), which we cannot obtain directly. To find the magnitude of the tangential force, we have to apply Newton's first law of motion, which states that the sum of all forces acting on an object is equal to zero. By applying this rule, we can determine the magnitude of the tangential force to achieve equilibrium.

Chapter 5

Wind Farms

When dealing with kites for energy production, it is crucial to consider the take-off and landing procedures. This is especially important for avoiding collisions and coordinating the take-off of multiple kites simultaneously to maximize energy output. This concept is fundamental in the development of wind farms.

Traditional wind farms are specific areas where wind turbines are grouped together to convert wind energy into electricity. These turbines need to be located in areas with consistent wind flow, away from large structures, to efficiently harness wind power [43].

There are two types of wind farms: offshore and onshore. Offshore wind farms are located far from the coast, in the ocean. These farms can accommodate large structures, and the turbines in this system have high capacity. Additionally, the wind in these regions is stronger and faster due to the absence of vertical barriers, whether natural or artificial [43]. Onshore wind farms, on the other hand, are located on the mainland. Most of the time, these farms are installed in rural areas at high altitudes, similar to the case in Portugal. They utilize wind turbines to convert energy [43].

In addition to traditional wind farms with turbines, there are ongoing studies to implement airborne wind energy and create wind farms using kites. These studies aim to determine the optimal number of kites needed to maximize energy production without compromising safety. Safety measures are crucial from the take-off of the kite to its entry into the flight envelope. Various take-off methods have been detailed in this document, each with specific conditions for coordinating multiple kites.

We will carry out a brief analysis of the impact that the various take-offs have when we are talking about Wind Farms. The first take-off to be analyzed is the horizontal one. In the horizontal take-off, the prototype is accelerated horizontally until the necessary speed is reached to start flying and producing energy. Analyzing the way this type of take-off is carried out, we can consider that there is no danger of collisions for the coordination of several kites. The most challenging aspect we need to consider is positioning the kites at the appropriate distance from one another. This ensures that when a kite enters the flight envelope, it does not collide with another kite that is also entering the same space. However, this type of approach for Wind Farms would probably not be the best option, since this type of take-off requires a lot of space and auxiliary equipment to allow

it to accelerate, which would take up a lot of space. As we want to maximize production with as many kites as possible in as little space as possible, this approach would take up a lot of space and the number of kites would be reduced.

The next take-off method to be examined is vertical take-off. Vertical take-off and landing (VTOL) involves using support propellers to help the kite or wing take-off vertically until the power generation process begins. Vertical take-off presents a minimal risk when coordinating multiple kites, as the kites slowly ascend in a vertical direction until they enter the flight envelope. Similar to horizontal take-off, multiple kites can ascend simultaneously with no risk of collision. The key consideration here is ensuring that when the kites enter the energy production phase and flight envelope, they are at a safe distance from one another. This type of take-off presents an interesting approach to maximizing production and minimizing kite space to accommodate as many units as possible.

Upon closer examination the take-off method under analysis in this thesis, which involves pendulum-based movement, it is essential to consider several key factors. Firstly, the implementation of this approach necessitates a physical structure, such as the existing turbine towers, to facilitate its operation. It is worth noting that this concept could potentially repurpose disused towers from decommissioned turbines, effectively breathing new life into otherwise overlooked structures. In contrast to horizontal and non-pendulum-based vertical take-off methods that require a designated space for the kite to move safely within the envelope and during energy production, using turbine towers as anchoring points eliminates these spatial concerns. Additionally, given that wind turbines within a farm must adhere to predefined minimum distances from one another, utilizing these towers to suspend multiple kite units provides sufficient space, ensuring the safe operation and non-interference of the kite units. However, this type of take-off is not only dependent on the existing turbine structures. It can also be used, for example, on a platform that can be designed and created for this purpose. This type of take-off is not exclusively for giving new life to turbines, but also serves as an important advantage.

In the diagram depicted in Figure 5.1, we observe the arrangement and spacing of turbines in a wind park, along with the prevailing wind direction. It is crucial to consider this wind direction when determining the optimal positioning of the kite to harness the speed of the wind effectively. In a wind farm with turbines, the typical distances between turbines are 5 to 9 times the rotor diameter in the prevailing wind direction, and 3 to 5 times the rotor diameter in the orthogonal direction.

One interesting possibility is to install kite units that use a pendulum movement for take-off, as proposed in this thesis, to generate energy alongside traditional turbines. This approach would involve harnessing two different methods of energy production to maximize output. However, it would be challenging to install these units on working turbines due to the size of the turbine blades and their movement. Factors such as minimum rope size for the kite, wind direction, kite layout, and weather conditions would all need to be carefully considered. Despite these challenges, implementing this approach could be a significant step forward, as it would allow for the utilization of space above ground level for energy production in addition to the ground-based turbines and

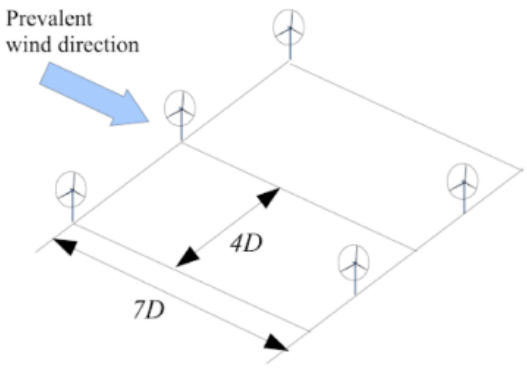


Figure 5.1: Turbines disposition. (Source: [19]

kite units.

The circular take-off and landing method involves the kite gradually increasing its speed while making circular movements until it reaches the necessary height to produce energy. This type of take-off requires the most attention when coordinating multiple kites to avoid collisions. Since the kite is increasing its speed by moving in circles, it is crucial to coordinate the kites to prevent collisions and minimize the space they occupy. Establishing minimum distances between kites is essential. Ideally, the kites should share a common area, as depicted in figures (5.3) and (5.4), rather than if they did not share as shown in figure (5.2). This usage of shared space allows for more efficient utilization and maximized production.

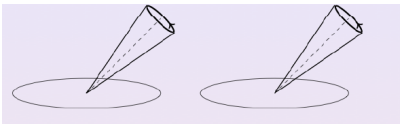


Figure 5.2: (i) Disjoint ground areas

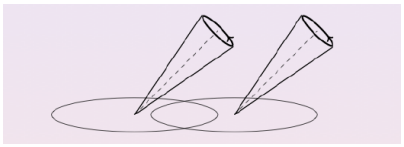


Figure 5.3: (ii) Disjoint workspace cones

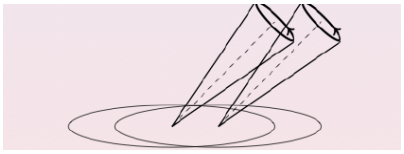


Figure 5.4: (iii) Intersecting workspace cones

Figure 5.5: AWES sharing a common space. (Source: [19])

It is important to consider various strategies, such as defining distances and controlling the inclination of the kite.

One of the strategies to be considered is determining the minimum distances required for this type of take-off on Wind Farms. The UPWIND group is also researching the use of kites on wind farms. In the study conducted to calculate the minimum distances required, a rectangular

layout was used with the configuration shown in figure 5.6, where multiple kite units operate in the upwind direction synchronously. The decision variable is the number of kites (denoted as n) to be placed in order to obtain the average power per cycle matrix n x P_c.

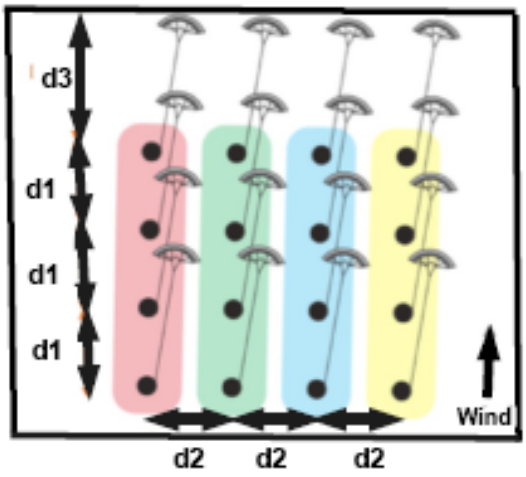


Figure 5.6: Kite disposition in a Wind Farm using a rectangular layout. (Source: [19]

With regard to the distances visible in figure 5.6, three minimum distances are established to ensure the safety of kites using circular take-off. These distances can be examined more closely in figures 5.7 and 5.8, and can be calculated using mathematical and physical considerations.

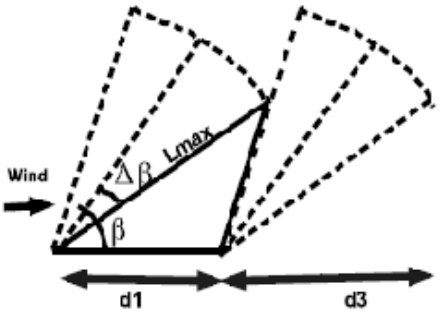


Figure 5.7: Distance 1 and 3.

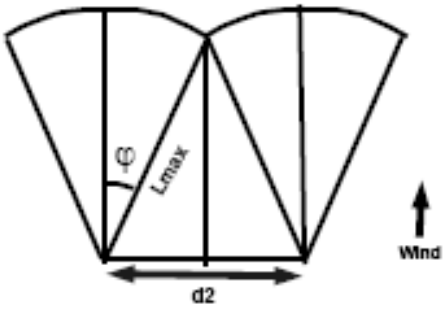


Figure 5.8: Distance 2.

Figure 5.9: Distances. (Source: [19])

The distance d_1 represents the distance between two points aligned with the wind velocity. It can be calculated using the formula 5.1 shown, which is based on the observation of the figure 5.7.

$$d_1 = \frac{L_{\max}}{\sin(\beta - \Delta\beta)[\frac{1}{\tan(\beta - \Delta\beta}} + \frac{1}{\tan(\beta + \Delta\beta]} \tag{5.1}$$

The next distance that must be accounted for is d_2, which represents the minimum distance between units when sketched from a top view to avoid interference. This can be calculated using the formula shown in 5.2.

$$d_2 = 2 \cdot L_{\max} \cdot \sin(\phi) \tag{5.2}$$

The final distance to calculate is denoted as d3. This distance represents the space between the last unit and the edge of the terrain in each column, aligned with the wind direction. It can be determined using the formula referenced in equation 5.3.

$$d_3 = L_{max} \cdot cos(\beta - \Delta\beta) \tag{5.3}$$

However, it does not include the maximum distance d, which is simply the larger of the distances d_1 and d_2, denoted as max(d_1, d_2). The distance d_3 does not appear in the calculation of the maximum distance d. When calculating these minimum distances, it is important to consider certain restrictions, such as the maximum altitude, the maximum and minimum elevation angles, as well as the length and width of the area where the wind farm is to be installed.

Distance calculations were conducted using real data collected as part of the UPWIND project. In figure 5.10, there is a table displaying the collected data, and in figure 5.11, the results of the distance calculations are presented.

Results					beta0 = beta (degree)	variação delta = azimuth		Lmax (m)	Pac cycle (w)	Number of Units
	1	2	3	4	5	6	7	8	9	10
1	0,9506	0,0014	0,5778	0,0430	38,7638	-643 282	15,7778	152,15074	248694,77136	1950,0
2	0,9458	0,0085	0,8843	0,0138	38,6444	-381 768	18,8434	150,69067	576932,85379	1950,0
3	0,9346	0,0084	0,5126	0,0074	38,3659	-386 881	15,1263	150,37145	1113444,83648	1950,0
4	0,9221	0,0038	0,7030	0,0066	38,0521	-555 624	17,0303	150,33089	1903803,10035	1950,0
5	0,9476	0,0013	0,5795	0,0352	38,6908	-645 473	15,7950	151,75963	2753574,06736	1950,0
6	0,9358	0,0020	0,8549	0,0251	38,3951	-621 732	18,5486	151,25564	3210622,28126	1950,0
7	0,9989	0,0036	0,4363	0,0843	39,9730	-561 468	14,3625	154,21305	3284746,87551	1950,0
8	0,9980	0,0266	0,9108	0,0364	39,9507	276 033	19,1079	151,81927	3229537,87022	1950,0
9	0,9949	0,0349	0,4562	0,0205	39,8717	580 646	14,5622	151,02581	3166221,18634	1950,0
10	0,9858	0,0297	0,6949	0,0216	39,6437	389 624	16,9489	151,07819	3106574,71908	1950,0
11	0,9997	0,0222	0,7482	0,0492	39,9930	115 692	17,4824	152,46086	3064323,11234	1950,0
12	0,9895	0,0216	0,2942	0,0370	39,7364	95 239	12,9417	151,84731	3002559,57937	1950,0
13	0,9908	0,0221	0,8270	0,0297	39,7688	112 039	18,2703	151,48338	2947227,71455	1950,0
14	0,9942	0,0311	0,9467	0,0196	39,8559	440 757	19,4672	150,98164	2892536,66520	1950,0
15	0,9986	0,0309	0,6445	0,0275	39,9640	433 453	16,4449	151,37349	2844988,34367	1950,0
16	0,9861	0,0085	0,5484	0,0544	39,6518	-383 959	15,4840	152,72033	2798268,04760	1950,0

Figure 5.10: Table with data from the studies of the UPWIND project.

The UPWIND group has established specific conditions to ensure safe distancing, as outlined in the equation provided in 5.4.

$$C_{CTOL} + \frac{b}{2} \leq \frac{d}{2} \tag{5.4}$$

Where b represents the size of the wing in meters and its value is already defined as b = 1.39. This allows us to calculate C_{CTOL}, which represents the maximum distance for the circular take-off. We also established another condition in which the distance d had to be greater than $4\dot{b}$, which states the maximum necessary distance.

Upon analyzing the results, it is evident that the distance d always equals d_1, which is the maximum distance and consistently the greatest distance. Evaluating the relative conditions $4\dot{b}$, which represents the maximum necessary distance, and given that b = 1.39, it is confirmed that we

Results										
m	d1	d2	d3	d	tan(x+y)	tan(x-y)	sen(x-y)	sen(x)	cos(x-y)	Lmax
1	117.0724	52,9150	133,3951	117.0724	1,1414	0,5486	0,4810	0,1739	0,8767	152,1507
2	116.1066	52,7779	132,3561	116.1066	1,1395	0,5443	0,4781	0,1751	0,8783	150,6907
3	115,6210	52,6571	132,4216	115,6210	1,1283	0,5380	0,4738	0,1751	0,8806	150,3715
4	115,2486	52,4054	132,7166	115,2486	1,1141	0,5320	0,4697	0,1743	0,8828	150,3309
5	116,8415	52,7759	133,1433	116,8415	1,1384	0,5470	0,4799	0,1739	0,8773	151,7596
6	116,2081	52,6339	133,0823	116,2081	1,1269	0,5401	0,4753	0,1740	0,8799	151,2556
7	119,9935	53,7494	133,6380	119,9935	1,1921	0,5759	0,4990	0,1743	0,8666	154,2131
8	118,5051	54,1114	131,8945	118,5051	1,2009	0,5701	0,4952	0,1782	0,8688	151,8193
9	117,9506	54,2606	131,4166	117,9506	1,2011	0,5663	0,4928	0,1796	0,8702	151,0258
10	117,6812	54,0074	131,6903	117,6812	1,1892	0,5623	0,4901	0,1787	0,8717	151,0782
11	118,9703	54,0504	132,3376	118,9703	1,2009	0,5720	0,4965	0,1773	0,8680	152,4609
12	118,2312	53,8633	132,1345	118,2312	1,1898	0,5662	0,4927	0,1774	0,8702	151,8473
13	117,9851	53,7584	131,7815	117,9851	1,1913	0,5669	0,4932	0,1774	0,8699	151,4834
14	117,8355	54,0454	131,3495	117,8355	1,1988	0,5668	0,4931	0,1790	0,8700	150,9816
15	118,2433	54,1766	131,5466	118,2433	1,2033	0,5694	0,4948	0,1790	0,8690	151,3735
16	118,5994	53,4857	132,8331	118,5994	1,1807	0,5673	0,4934	0,1751	0,8698	152,7203

Figure 5.11: Calculating distances for the presented data.

will not encounter any issues, as the distances for d mostly exceed 100 meters. In this scenario, we would not encounter issues with distances and collisions because the maximum distances and the distances required for the circular take-off are larger than needed. To optimize production and minimize the space used, we could consider installing additional kite units or larger kite units. However, these are just assumptions since these types of wind farms do not currently exist.

In addition to considering the distances, we also need to account for the inclinations of the kites. The angle that the kite makes with the ground, known as the β angle, can be more open or more closed. This angle affects the coordination lift times of the kites, which helps prevent collisions. We can coordinate several units taking into account the inclination. This can be useful when we have kite units sharing a significant common space and we want to avoid collisions. However, it also impacts energy production, as a larger inclination results in less energy production.

In brief, take-off is crucial not only for achieving full autonomy in a device, ensuring maximum efficiency and safety without human intervention, but also for enabling multiple kites to operate simultaneously in wind farms. The creation of this type of wind farms does not exist yet, but it could be a very good alternative to traditional wind farms with turbines. It would create a more pleasing view and take advantage of stronger winds at higher altitudes. Additionally, by controlling the space, we can have several units sharing a common space to maximize the output.

Chapter 6

Conclusions and Future Work

6.1 Conclusions

Although renewable energy has been growing, fossil fuels still make up the majority of the energy produced and used globally. It is essential to find sustainable solutions to reduce dependence on these unsustainable energy sources and take advantage of unlimited and economically efficient natural resources.

Airborne Wind Energy Systems can harness wind power to generate energy. Although still under development, this technology could become a viable and competitive energy production method in the future. The UPWIND project focuses on researching and developing AWES that use a kite or wing, a cable, and a generator to produce energy through high-altitude traction. Developing an automatic take-off and landing controller is a crucial step in making these systems more independent, improving their efficiency and autonomy.

However, controlling these systems automatically involves managing several parameters and understanding the kinematic and dynamic model of the kite. The chosen take-off and landing method is also a crucial factor to consider.

The UPWIND project is exploring alternative and innovative methods that have great potential to bring about significant advancements, such as take-off based on a pendulum movement. However, there are also major control problems that need to be addressed.

In this document, we conducted simulations on a range of problems with different levels of complexity. These included studying the movement of a simple pendulum and the kite in a 3D perspective, as well as studying and developing a kite controller using 2D pendulum movement.

Through observation, we can conclude that the results obtained in the 2D perspective achieve good results considering the conditions used, and show promising advantages of this type of technology. The 3D study provides a great background of the dynamics and mathematical relationships that can be used for further development of the controller under these conditions.

In conclusion, the main goal of this dissertation was to create an automated take-off and landing controller capable of achieving high levels of autonomy and efficiency.

6.2 Future Work

In future work, it would be interesting to use this thesis as a starting point for a more comprehensive study of take-off using pendulum movement. It would be interesting to implement and obtain the results of simulations for the 3D model. This will allow us to observe what happens when the wind is perpendicular to the position of the kite and to compare these results with those obtained in the 2D model. In both 3D and 2D perspectives, it would be interesting to use real-time factors to observe the influence on the motion of the kite and the graphics. In the 2D perspective, conducting more studies while taking into account all the forces acting on the kite, not just the ones directly affecting the motion, such as the push force and the drag force, would also be beneficial. It is important to study what happens after the kite achieves the necessary speed and enters a steady state of circular movement, such as how the kite would enter the flight envelope to start producing energy. Understanding how the kite would move for that, and where the wind should strike to help or hinder the ascent of the kite, is crucial. It would also be important to examine the context of the take-off, where the kite is suspended from a tower, and conduct a study on how the kite would land safely without hitting the tower or landing unbalanced. Given that this is a completely innovative context, there are several factors to take into account from the moment of take-off to the moment of landing in order to make this a viable and safe option. Further development of this type of take-off could also explore how it would interact with wind farms.

Suspended by a cable, this type of take-off could potentially repurpose turbines that are out of service, but this type of take-off is not only dependent on the turbines. It would be interesting to study the design or the projecting of specific structures that are designed for this type of take-off, which could enhance its effectiveness. Another interesting aspect would be to analyze the viability and the possibility of having a kite perform the pendulum take-off on working turbines. This is important to analyze due to the fact that in working turbines, we have the blades working, which could possibly lead to disasters and make it very difficult to have the two systems operating. However, it would be interesting to consider a possibility where this could be successful.

In summary, this type of take-off has significant potential, and this thesis could serve as a foundation for more in-depth studies and simulations on it, exploring the entire flight cycle from take-off to landing.

References

[1] United Nations. Teaching sustainable development goals. https://www.un.org/pt/teach/SDGs.

[2] AWESCO. Airborne wind energy system modelling, control and optimisation. https://awesco.eu/awe-explained/, 2024.

[3] Stephanie Mann. An introduction to airborne wind. 2019. https://ore.catapult.org.uk/analysisinsight/an-introduction-to-airborne-wind/(visited on 2023-06-02).

[4] Zahra Ramin, Mozafar Rahimi, and Reza S. Bozorgi-Amiri. The impact of demand response on the power generation expansion planning with high penetration of renewable energy. *Renewable and Sustainable Energy Reviews*, 51:153–163, 2015.

[5] Moritz Diehl. Airborne Wind Energy: Basic Concepts and Physical Foundations. In Uwe Ahrens, Moritz Diehl, and Roland Schmehl, editors, *Airborne Wind Energy*, pages 3–22. Springer Berlin Heidelberg, Berlin, Heidelberg, 2013. Series Title: Green Energy and Technology.

[6] AWESCO. Airborne wind energy explained. https://awesco.eu/awe-explained/, 2024.

[7] Paul Dvorak. Power from parachutes, wings, kites, and more: A review of the technologies, March 22 2018.

[8] Lorenzo Fagiano, Manfred Quack, Florian Bauer, Lode Carnel, and Espen Oland. Autonomous airborne wind energy systems: Accomplishments and challenges. *Annual Review of Control, Robotics, and Autonomous Systems*, 5(1):603–631, May 2022.

[9] Kitemill. Kitemill buys kps, July 11 2024.

[10] TwingTec AG. TwingTec Website, 2024.

[11] Alameda Point Environmental Report. Makani, 2024.

[12] Jaap Bosch. Future of airborne wind energy systems depends on safety and efficiency. *Windpower Engineering Development*, September 12 2022.

[13] Ricardo Albarracín Sánchez, María Teresa Fernández García, Manuel Romero Gómez, Domingo Gómez García, Francisco Javier Molina López, and Juan Manuel Andújar Márquez. A comprehensive review of wireless power transfer for electric vehicles: Past, present, and future trends. *Energies*, 15(7):2502, 2022.

[14] Gabriel Moura Fernandes. Take-off and landing of autonomous flying wings in airborne wind energy systems. Master's thesis, FEUP, 2023.

[15] Energie-Experten. Enerkite lenkdrachen versorgt 60 haushalte mit strom, 2020.

[16] Freepik. Aviao em fundo branco ilustracao 3d isolada, 2024.

[17] ResearchGate. Figura 1: Representação do pêndulo simples no instante inicial e das forças que atuam, 2024.

[18] Chris Vermillion, Mitchell Cobb, Lorenzo Fagiano, Rachel Leuthold, Moritz Diehl, Roy S. Smith, Tony A. Wood, Sebastian Rapp, Roland Schmehl, David Olinger, and Michael Demetriou. Electricity in the air: Insights from two decades of advanced control research and experimental flight testing of airborne wind energy systems. *Annual Reviews in Control*, 52:330–357, January 2021.

[19] Luís A.C. Roque, Luís Tiago Paiva, Manuel C.R.M. Fernandes, Dalila B.M.M. Fontes, and Fernando A.C.C. Fontes. Layout optimization of an airborne wind energy farm for maximum power generation. *Energy Reports*, 6(Supplement 1), 2020.

[20] Uwe Ahrens. *Airborne Wind Energy: An Overview of the Technological Approaches*. Green Energy and Technology. Springer International Publishing, Cham, 2023.

[21] André F. C. Pereira and João M. M. Sousa. A review on crosswind airborne wind energy systems: Key factors for a design choice. *Energies*, 16(1):351, January 2023.

[22] Paul Williams, Marcos Paz, Michiel Kruijff, and Durk Steenhuizen. Autonomous takeoff and landing of rigid wing airborne wind energy systems. *8th Airborne Wind Energy Conference (AWEC 2019)*, 2019.

[23] Sven Jackisch. Automatic and runway-independent take-off and landing system for solar-electric flight of medium-weight uavs. https://www.fsd.rwth-aachen.de/cms/fsd/Forschung/Projekte/ nnrrz/ElektRail/lidx/1/(visited on 2023-06-02).

[24] John D Anderson. *Fundamentals of Aerodynamics*. McGraw-Hill Education, New York, USA, 6th edition, 2016.

[25] M L Loyd. Crosswind kite power. *Journal of Energy*, 4(3):106–111, 1980.

[26] Thomas Ackermann. *Airborne Wind Energy: Advances in Technology Development and Research*. Springer, Cham, Switzerland, 2021.

[27] Lorenzo Fagiano, Mario Milanese, and Dario Piga. Design and model-based control of a high-altitude wind power system. In *2013 American Control Conference*, pages 3839–3844. IEEE, 2013.

[28] Alessandro Cherubini, Anna Papini, Rocco Vertechy, and Marco Fontana. Airborne wind energy systems: A review of the technologies. *Renewable and Sustainable Energy Reviews*, 51:1461–1476, 2015.

[29] Tobias Arndt, Stefan Emeis, Gerd Jacobs, and Roland Schmehl. Airborne wind energy: an overview. *Journal of Physics: Conference Series*, 524(1):012138, 2014.

[30] Roland Schmehl, Samantha Watson, and Richard van der Vlugt. *Concepts and Technologies for Airborne Wind Energy*, volume 166. Springer, 2013.

[31] John D Anderson. *Introduction to Flight*. McGraw-Hill, 2001.

[32] Brian L Stevens and Frank L Lewis. Aircraft control and simulation. *AIAA education series*, 2003.

[33] Howard D Curtis. *Fundamentals of Aircraft Structural Analysis*. McGraw-Hill Science/Engineering/Math, 2010.

[34] Angelo Miele. Flight mechanics. *Journal of Guidance, Control, and Dynamics*, 18(6):1329–1337, 1995.

[35] Arturo Tadeo Espinoza-Fraire, Alejandro Enrique Dzul López, Ricardo Pavel Parada Morado, and José Armando Sáenz Esqueda. Equations of motion of a fixed-wing uav. In Arturo Tadeo Espinoza-Fraire, Alejandro Enrique Dzul López, Ricardo Pavel Parada Morado, and José Armando Sáenz Esqueda, editors, *Design of Control Laws and State Observers for Fixed-Wing UAVs*. Elsevier, 2023.

[36] Herbert Goldstein, Charles P Poole, and John L Safko. *Classical Mechanics*. Pearson Education, 2002.

[37] Daniel Kleppner and Robert J Kolenkow. *An Introduction to Mechanics*. Cambridge University Press, 2013.

[38] Jerry B Marion and Stephen T Thornton. *Classical Dynamics of Particles and Systems*. Cengage Learning, 2004.

[39] Manuel Côrte-Real de Matos Fernandes. Airborne wind energy systems: Modelling, simulation and economic analysis. Master's thesis, FEUP, 2018.

[40] MathWorks. Ordinary differential equations. https://www.mathworks.com/help/matlab/ordinary-differential-equations.html.

[41] MathWorks. ODE45 (Ordinary Differential Equation Solver), 2024.

[42] Manuel C.R.M. Fernandes, Luís Tiago Paiva, and Fernando A.C.C. Fontes. Power production. *SYSTEC, Faculdade de Engenharia, Universidade do Porto*.

[43] GoldEnergy. Parque eólico, 2024.